# International Ocean Discovery Program Expedition 402 Scientific Prospectus

## Tyrrhenian Continent–Ocean Transition

## Tyrrhenian Magmatism and Mantle Exhumation (TIME)

**Nevio Zitellini**
**Co-Chief Scientist**
Institute of Marine Science (ISMAR)
Consiglio Nazionale delle Ricerche
Italy

**Alberto Malinverno**
**Co-Chief Scientist**
Lamont-Doherty Earth Observatory
Columbia University
USA

**Emily R. Estes**
**Expedition Project Manager/Staff Scientist**
International Ocean Discovery Program
Texas A&M University
USA

## Publisher's notes

This publication was prepared by the *JOIDES Resolution* Science Operator (JRSO) at Texas A&M University (TAMU) as an account of work performed under the International Ocean Discovery Program (IODP). This material is based upon work supported by the JRSO, which is a major facility funded by the National Science Foundation Cooperative Agreement Number OCE1326927. Funding for IODP is provided by the following international partners:

National Science Foundation (NSF), United States
Ministry of Education, Culture, Sports, Science and Technology (MEXT), Japan
European Consortium for Ocean Research Drilling (ECORD)
Ministry of Science and Technology (MOST), People's Republic of China
Australia-New Zealand IODP Consortium (ANZIC)
Ministry of Earth Sciences (MoES), India

Portions of this work may have been published in whole or in part in other IODP documents or publications.

This IODP *Scientific Prospectus* is based on precruise *JOIDES Resolution* Facility advisory panel discussions and scientific input from the designated Co-Chief Scientists on behalf of the drilling proponents. During the course of the cruise, actual site operations may indicate to the Co-Chief Scientists, the Expedition Project Manager/Staff Scientist, and the Operations Superintendent that it would be scientifically or operationally advantageous to amend the plan detailed in this prospectus. It should be understood that any substantial changes to the science deliverables outlined in the plan presented here are contingent upon the approval of the IODP JRSO Director and/or *JOIDES Resolution* Facility Board.

### Disclaimer



### Copyright



### Citation

Zitellini, N., Malinverno, A., and Estes, E.R., 2023. Expedition 402 Scientific Prospectus: Tyrrhenian Continent–Ocean Transition. International Ocean Discovery Program. https://doi.org/10.14379/iodp.sp.402.2023

### ISSN

World Wide Web: 2332-1385

March 2023

# Abstract

A tenet of plate tectonics is that divergent plates cause the asthenospheric mantle to ascend, decompress, and melt, producing new magmatic crust. However, drilling west of Iberia in the 1980s discovered a continent–ocean transition (COT) made of exposed mantle, revising models of lithospheric thinning and melt generation and defining magma-poor margins. A long-standing argument about mantle in COTs concerns its nature as either subcontinental or being exhumed during ultraslow seafloor spreading. Additionally, two models attribute the apparent lack of melts either to slow extension resulting in low ascent rates with enhanced asthenospheric cooling and reduced melt production or to upwelling mantle originally too depleted to produce a significant melt fraction. The debate on COT models is limited by the scarce evidence obtained in ultra-deepwater drilling, restricted to a few basement highs. Thus, 30 y after its discovery, the nature and genesis of COTs is still controversial. The comparatively shallow water depth and thin sediment cover of the Tyrrhenian Sea provide an optimal location to test COT formation models by drilling. The Tyrrhenian is the only example where extensive modern geophysical data has accurately mapped basement domains of a conjugate pair of COTs. They can be characterized with unprecedented detail in a single drilling expedition to study the time and space evolution of COT processes. Expedition 402 will drill two perpendicular transects. An east–west transect will target the progression from magmatic crust to exhumed mantle; a north–south transect will map the fault zone that exhumed the mantle. Drilling will sample the complete sediment section including Messinian deposits, the sediment/basement interface, the mantle, the associated magmas, and the products of syntectonic, and possibly ongoing, fluid-rock interactions to evaluate the hydrosphere–lithosphere geochemical exchange and potential related ecosystems.



# Plain language summary

The discovery in the 1980s of exposed mantle in the continent–ocean transition west of Iberia started an ongoing debate on the mechanisms of lithospheric extension and mantle exhumation, on the definition of continental break-up and initial seafloor spreading, on the nature of the continent–ocean transition, and on the first emplacement of oceanic crust. Our imperfect understanding of continent–ocean transition processes and of the onset of seafloor spreading is largely due to the worldwide limitation on drilling basement rocks typically buried under several kilometers of sediments. There are four main reasons to drill the Tyrrhenian Basin: it is very young and consequently has a thin sedimentary cover; its bedrock lithology and stratigraphy is extremely well documented by more than 40 y of academic investigations; a 30 m section of partially serpentinized peridotite has been already recovered in the center of the basin; and extensive recent seismic refraction and reflection experiments suggest that most of the basement in the center of the Tyrrhenian is made of exhumed mantle. Expedition 402 will drill two perpendicular transects. An east–west transect will target the progression from magmatic crust to exposed mantle; a north–south transect will map the fault zone that exhumed mantle. Drilling will sample the mantle, the associated magmas, and the products of syntectonic, and possibly ongoing, fluid-rock interaction to evaluate the geochemical exchange between the lithosphere and the hydrosphere and potential related ecosystems.


# 1. Schedule for Expedition 402

International Ocean Discovery Program (IODP) Expedition 402 is based on IODP drilling Proposal 927 (available at **https://iodp.tamu.edu/scienceops/precruise/tyrrhenian/927-Full2_Zitellini_web.pdf**). Following evaluation by the IODP Scientific Advisory Structure, the expedition was scheduled for the research vessel (R/V) *JOIDES Resolution*, operating under contract with the *JOIDES Resolution* Science Operator (JRSO). At the time of publication of this *Scientific Prospectus*, the expedition is scheduled to start in Naples, Italy, on 9 February 2024 and to end in Naples on 8 April 2024. A total of 59 days will be available for the transit, drilling, coring, and downhole measurements described in this report (for the current detailed schedule, see

**https://iodp.tamu.edu/scienceops**). Further details about the facilities aboard *JOIDES Resolution* can be found at **https://iodp.tamu.edu/labs/index.html**.

## 2. Introduction

A tenet of plate tectonics is that divergent plates cause asthenospheric mantle to ascend and melt by decompression, producing new basaltic ocean crust. However, drilling west of Iberia discovered a continent–ocean transition (COT) made of exposed mantle (Boillot and Winterer, 1988; Shipboard Scientific Party, 1973), prompting the revision of current models of lithospheric thinning and melt generation and the definition of magma-poor margins. A long-standing argument about mantle of COTs concerns its nature as either subcontinental or exhumed by ultraslow seafloor spreading. Additionally, two models explain the apparent lack of melts by invoking either slow extension resulting in low ascent rates, enhanced asthenospheric cooling, and reduced melt production or an upwelling mantle originally too depleted to produce significant amounts of melt. These debates on COT models persist due to the limited evidence recovered by drilling, which is restricted to a few basement highs. Thus, 30 y after its discovery we still debate on the nature and genesis of COTs. IODP Expedition 402, The Tyrrhenian Magmatism and Mantle Exhumation (TIME) project, tackles those issues.

The young Tyrrhenian Basin was formed by rifting during the eastward migration of the Calabrian arc. It is bounded eastward by the Italian peninsula and westward by Corsica and Sardinia. Modern investigations support a rapid continental break-up in the Tyrrhenian, giving birth first to a segment of new magmatic crust with the layered seismic structure of oceanic crust, followed by the exposure of segments of exhumed mantle with discrete basaltic intrusions. This sequence of events is at odds with current COT models.

Our main hypothesis is that the spatial variability of tectonic and magmatic structure in the Tyrrhenian may be present elsewhere but that paucity of both basement sampling and modern geophysical work have unduly affected conventional wisdom. This hypothesis can be tested only by drilling to determine the nature of the basement rocks and quantify the extension rates.

To test the hypothesis, Expedition 402 will drill two perpendicular transects (Figure **F1**). The east–west transect targets the progression from magmatic crust to exhumed mantle; the north–south transect maps the fault zone along which mantle is exhumed. Drilling will sample the mantle, the associated magmas, and the products of syntectonic, and possibly ongoing, fluid-rock interaction to evaluate the hydrosphere–lithosphere geochemical exchange and potential related ecosystems.

## 3. Background

The discovery of exposed mantle in the COT west of Iberia (Boillot and Winterer, 1988; Shipboard Scientific Party, 1973) triggered an ongoing debate on the mechanisms of lithospheric extension and mantle exhumation, the definition of break-up and initial seafloor spreading, and the nature of the COT and first oceanic crust. Our limited understanding of COT processes and of the onset of seafloor spreading is largely caused by the inability to drill deeply buried COT basement under deep waters at several worldwide locations. Current COT models are based on a few submarine examples and extrapolation from regionally restricted land analogs outcropping in highly deformed mountain belts.

The formation of magma-poor COTs is currently described by a succession of processes: following break up, mantle is exhumed first, gradually exposing deeper lithospheric levels until eventually a shoaling asthenosphere produces melt (e.g., Pérez-Gussinyé et al., 2006; Davis and Lavier, 2017; Gillard et al., 2017). However, that idealized sequence has not been convincingly found by sampling in any COT, and remains a conceptual model based on fragmentary sampling and seismic imaging without detailed constraints on the velocity structure.

Growing evidence suggests that conventional COT models are inadequately constrained by the limited drill information. During the last ~15 y, improved observational quality called for a revi-

sion of COT models. Regional geophysical data from the Woodlark Basin (Goodliffe and Taylor, 2007) and the northwest South China Sea Basin (Cameselle et al., 2017) support magma-poor rifting; however, break up was shortly followed by seafloor spreading with no mantle exhumation. Similarly, intense magmatism followed rapid breakup in the Gulf of California (Lizarralde et al., 2007), whereas the Black Sea Basin displays abrupt lateral changes from magma-poor to magma-rich COTs (Shillington et al., 2009). Ocean Drilling Program (ODP) drilling in the Woodlark Basin focused on continental faulting rather than the COT, and the Black Sea and Gulf of California basements are deep and unsampled. Only recently IODP drilling confirmed a sharp COT in the northwest South China Sea (Larsen et al., 2018).

Those studies highlight the end-member character of current conceptual COT models, which are based on a few Atlantic-type margins whose structure was mapped with vintage low-resolution geophysics. For instance, the boundary between exhumed mantle and oceanic crust west of Galicia is still undefined after >40 y of work. Similarly, the structure of the best conjugate pair of COTs sampled to date (West Iberia and Newfoundland) is inconclusively known. Interpretations of drilling results in the Iberia Abyssal Plain originally proposed >100 km exhumation of amagmatic continental mantle with no melt production (Shipboard Scientific Party, 1973), driving conceptual COT models. In contrast, the only modern wide-angle seismic (WAS) profile (but away from drilling transects) across the COT of the Deep Galicia margin that has higher spatial resolution (ocean-bottom seismometer [OBS] spacing ~15 km) than previous results (OBS spacing ~30 km) appears to detect patches of 0.5–1.5 km thick magmatic crust overlaying partially exhumed mantle (Davy et al., 2016). However, it is unclear whether existing drilling represents the regional COT

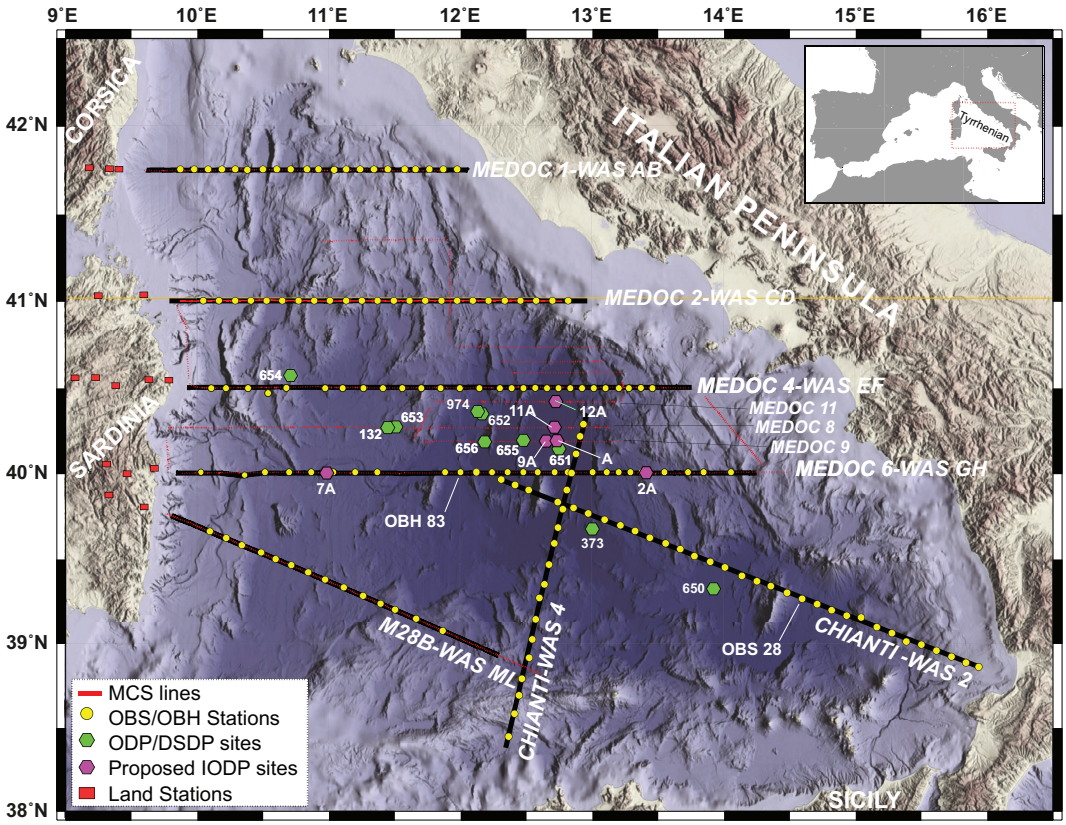


**Figure F1.** Bathymetric and topographic map of the Tyrrhenian region located in the western Mediterranean (see inset). Bathymetric data are downloaded from EMODnet portal (EMODnet Bathymetry Consortium, 2018), and topographic data are part of SRTM 90m data set freely available (**https://srtm.csi.cgiar.org**). The most relevant profiles for this study are MEDOC4/WAS EF Line (Prada et al., 2015) and MEDOC6/WAS GH Line (Prada et al.,2014) in the central Tyrrhenian Sea. OBH = ocean borehole seismometer. ODP and DSDP sites were sampled in the seventies and eighties (Ryan et al., 1970; Dietrich et al., 1977; Kastens and Mascle, 1990).

structure because drilling sampled shallow basement highs, where no oceanic crust occurs. Drilling the conjugate sector of the Newfoundland margin (with a reconstruction uncertainty of ~100 km) found limited synrift magmatism (Tucholke et al., 2007), supported by geophysical data (Hopper et al., 2004).

Therefore, new evidence about COT structures formed by the interplay of magmatic and tectonic processes indicates that end-member magma-poor models in the literature may be oversimplifications due to scarce drilling information. Furthermore, it is unclear whether the process of mantle unroofing consists of exhumation of continental lithosphere by depth-dependent differential stretching of the crust and mantle, a process that may involve little or no magmatism, or exhumation by slow to ultraslow seafloor spreading.

The comparatively better mapped Tyrrhenian basement (with seven WAS profiles across the basin and thousands of kilometers of seismic images) is at odds with the current view, showing that oceanic crust formation was followed by mantle exhumation while the opening rate remained nearly constant (Prada et al., 2016).

## 3.1. Geological setting

The Tyrrhenian was surveyed in the 1970s–1980s with thousands of kilometers of seismic reflection lines (Figure F2, inset), gravity and magnetic field measurements, heat flow measurements, dredge samplings (Figure F3), and drilling (Deep Sea Drilling Project [DSDP] Leg 13 Site 132

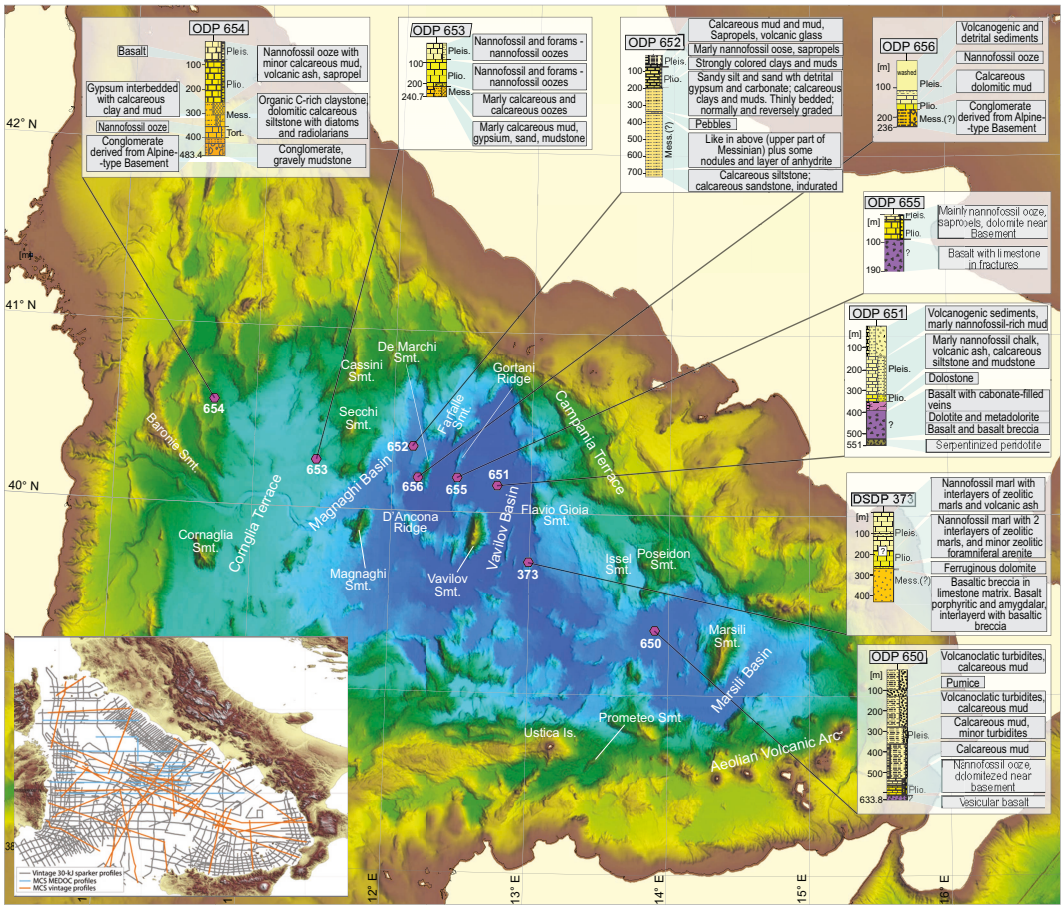


**Figure F2.** Bathymetric map of the Tyrrhenian Basin generated using middle-resolution data downloaded from the EMODnet portal (EMODnet Bathymetry Consortium, 2018). The location of DSDP (Ryan et al., 1970; Dietrich et al., 1977) and ODP (Kastens and Mascle et al., 1990) sites with their respective synthetized stratigraphic columns are indicated. Smt = seamount. Inset: location of vintage single-channel reflection lines (gray) and MCS reflection lines.

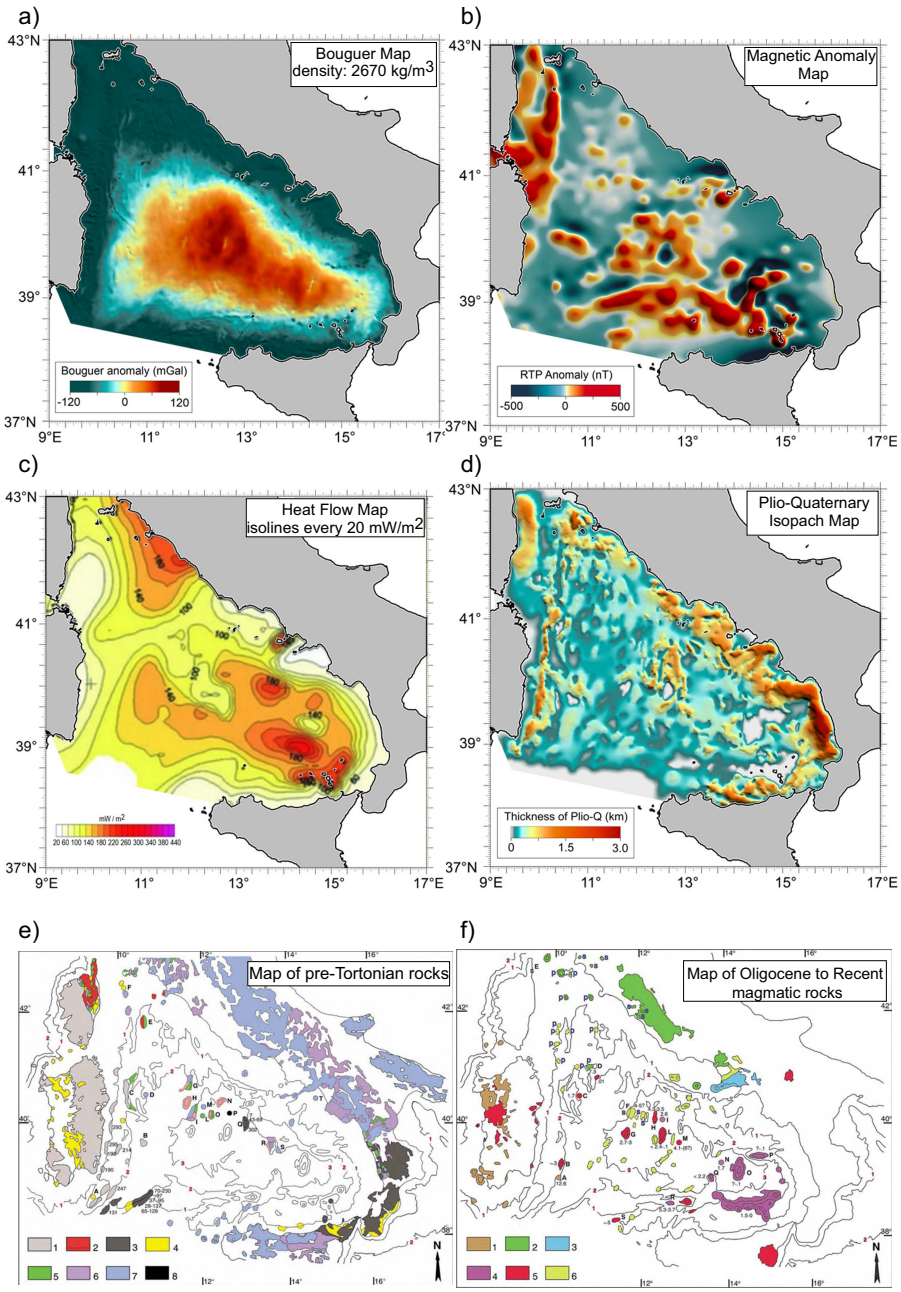


**Figure F3.** A. Bouguer anomaly from satellite-derived free air anomaly (Sandwell et al., 2014). Bouguer anomalies are obtained by subtracting from free air anomalies the attraction of seafloor topography and of unconsolidated sediments using a density contrast of 1630 Kg/m$^3$ and of 770Kg/m$^3$, respectively. B. Reduced to pole (RTP) magnetic anomaly of the aeromagnetic field (AGIP and SGN, 1994) from Caratori Tontini et al. (2004). C. Heat flow map of the Tyrrhenian region (Reproduced from Della Vedova et al., 2001. Deep temperatures and surface heat flow distribution. Springer, 65–76. doi: 10.1007/978-94-015-9829-3_7. By permission from SNCSC. Please visit: **https://link.springer.com/chapter/10.1007/978-94-015-9829-3_7**. This figure is not included under the Creative Commons CC-BY 4.0 license of this publication. For permissions, please email: Journalpermissions@springernature.com). D. Pliocene–Quaternary Isopach map of the Tyrrhenian Basin derived from a dense network of high-resolution, single-channel, seismic reflection profiles (Figure F1, inset). E. Map of the pre-Tortonian rocks distribution in the Tyrrhenian region with their radiometric ages (from Sartori, 2005). 1 = Variscan rocks, 2 = metamorphic units of Alpine Corsica, 3 = Calabride-Peloritanian-Kabilide units, 4 = Oligocene to Middle–Late Miocene sedimentary rocks, 5 = ophiolite of the Tethyan domain, 6 = Apenninic-Maghrebian units, 7 = carbonate sequence of Apenninic-Maghrebian units, 8 = central Tyrrhenian metamorphic rock of uncertain paleogeographic attribution. F. Distribution of Oligocene to recent magmatic rocks (from Sartori, 2005). 1 = Oligocene to Middle Miocene island arc basalts, 2 = Tortonian to recent rocks either with mantle sources contaminated by crustal materials or derived from upper crustal sources or derived by mixing between crustal and mantle sources (Tuscany and Latium on land), 3 = Pleistocene to recent rocks with OIB mantle sources enriched by subduction-related sources (Campania), 4 = Pliocene to recent rocks with island arc basalt type mantle sources, 5 = Pliocene to recent rocks derived from OIB-type and from MORB mantle sources, 6 = rocks from undefined magma sources.

[Ryan et al., 1970] and Leg 42 Site 373 [Shipboard Scientific Party, 1978] and ODP Leg 107 Sites 650–656 [Kastens and Mascle, 1990]). In the 1990s, the Tyrrhenian was mapped entirely with multibeam bathymetry and high-quality, deep penetrating, seismic data acquired on behalf of the Italian Crosta Profonda (CROP) program (Figure **F1**). In 2010, the Mediterranean overturning circulation (MEDOC) project acquired five geophysical transects across the basin with coincident WAS, gravity and multichannel seismic (MCS) reflection data, and additional MCS lines across the basin center (Prada et al., 2014). In 2015, the Calabrian Arc Hazards in Ionian and Tyrrhenian Seas (CHIANTI) project collected two WAS lines across the central-eastern basin (Prada et al., 2020) (see Figure **F1** for location).

The Tyrrhenian opened by stretching of ~300 Ma Variscan continental lithosphere, exposed in Corsica and Sardinia, driven by slab rollback of the east–southeast migrating Apennine subduction (Malinverno and Ryan, 1986; Faccenna et al., 2001). Significant extension started in the Late Miocene (~10 Ma), causing continental break up, a first phase of magmatism, and subsequent mantle exhumation in the Magnaghi-Vavilov Basin after the Messinian, between about 5 and 2 Ma (Prada et al., 2016).

The amount of extension increases from north to south, mirrored by seafloor morphology. The Tyrrhenian seafloor has three morphological domains (Figures **F1**, **F2**): A Northern Tyrrhenian region north of ~40°45′N, where the seafloor is shallow and rough; a Central Tyrrhenian region (40°45′N to ~39°30′N) with a deeper seafloor, sedimented plains with volcanoes like Magnaghi and Vavilov and nonvolcanic basement seamounts like Secchi, Farfalle, Flavio Gioia and De Marchi (Figure **F2**); and a Southeastern Tyrrhenian region (39°30′N to 38°N) with the Marsili Basin and volcano and the Aeolian volcanic arc.

The Northern Tyrrhenian shows north–south trending normal faults thinning the continental crust to 20–25 km (Mauffret et al., 1999; Moeller et al., 2013, 2014). The Central and Southeastern Tyrrhenian display increased extension (Figure **F4C, F4D**) with subbasins originally interpreted as continental (Cornaglia Terrace) or oceanic (Magnaghi, Vavilov, and Marsili Basins) (Duschenes et al., 1986; Kastens and Mascle, 1990; Sartori, 1990) with several kilometers tall volcanoes of upper Pliocene to present-day age (Argnani and Savelli, 1999; Savelli, 1988, 2002; Lustrino et al., 2011) (Figure **F3F**).

MEDOC *P*-wave velocity ($V_P$) models from WAS data show that the Cornaglia and Campania Terraces basement has the Layer 2/3 classical oceanic seismic structure, supporting magmatic accretion (Prada et al., 2014, 2015). Thus, $V_P$ models support a continental break-up followed (in the Tortonian/Messinian) by some 100–150 km wide magmatic construction in the Cornaglia and Campanian Terraces, possibly resembling the mid-ocean-ridge basalt (MORB) sampled at Site 373 (Figures **F2**, **F4C**). However, Site 373 does not unequivocally represent the Campanian Terrace basement because it is at its edge.

Further, MEDOC and CHIANTI $V_P$ models, supported by gravity modeling, seismic reflection images, and basement drilling indicate that the Magnaghi, Vavilov, and Marsili Basins are floored by exhumed mantle (Figure **F4A–F4C**) intruded by mid-ocean ridge (MOR)-type fissural volcanism (Prada et al., 2014, 2015), and later intraplate back-arc volcanism (Figure **F4E**) (Prada et al., 2016).

The basement of the Magnaghi-Vavilov Basin was recovered at ODP Sites 651 and 655 and DSDP Site 373 (Figure **F2**). All three sites recovered basalts with major element compositions similar to MORB and an enriched trace element pattern typical of enriched MORB (E-MORB) (Beccaluva et al., 1990). MORB at Site 651 is overlain by a basaltic unit with a back-arc basin (BAB)-like signature (Bertrand et al., 1990). The upper basaltic unit at Site 651 has major calc-alkaline affinity and shows enrichment in large ion lithophile element (LILE) and negative anomalies of high field strength elements (HFSE) (particularly Nb) (Bertrand et al., 1990). The high LILE/HFSE ratio of the younger unit indicates contamination from slab fluids during the last volcanic phase. These BAB-like volcanics may relate to the growth of the nearby Marsili Seamount, which was likely formed after extension ceased (Figure **F4E**) (Prada et al., 2016).

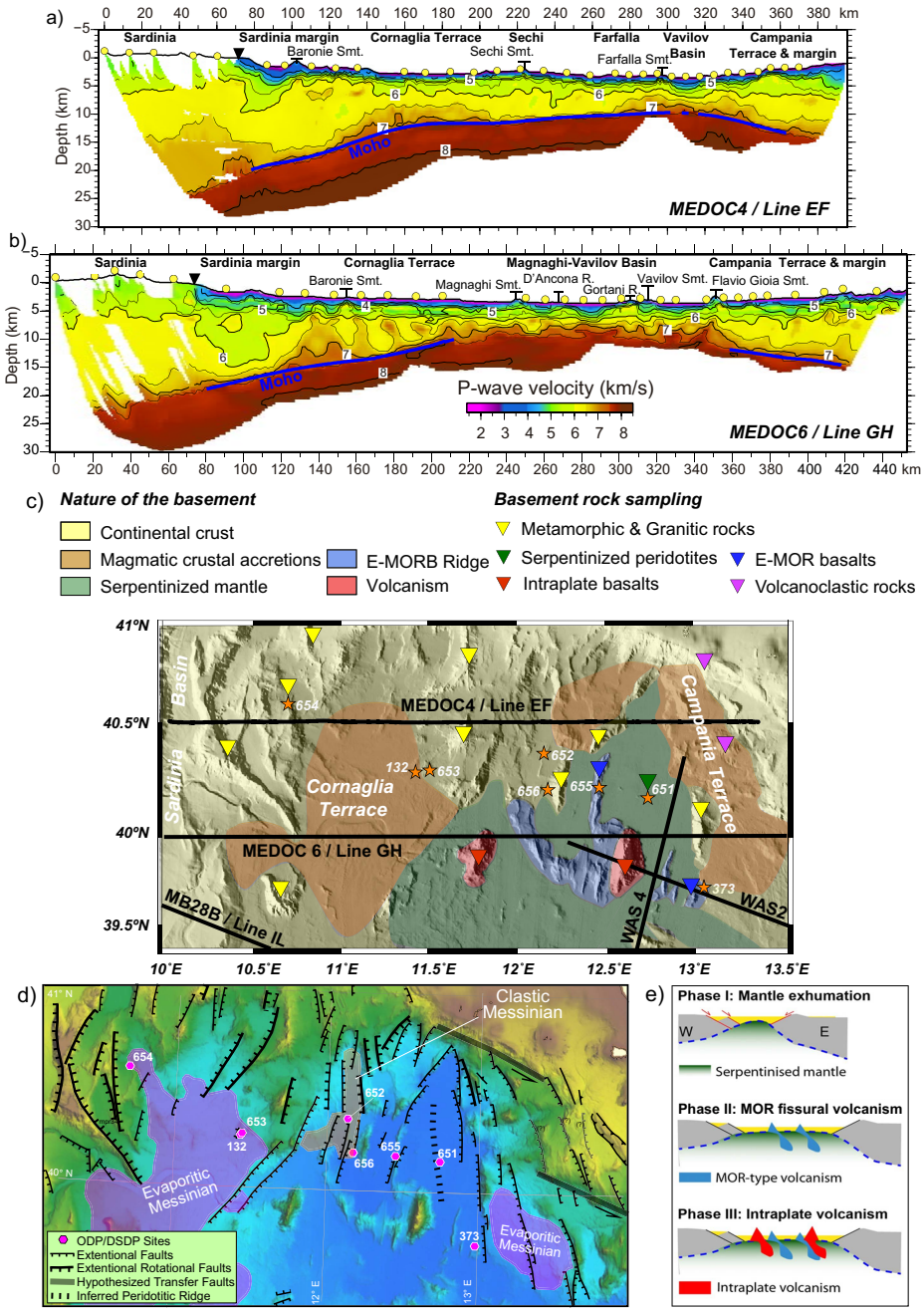


**Figure F4.** A, B. 2-D $V_P$ models of Transects (A) EF (reproduced from Prada et al., 2014. Seismic structure of the Central Tyrrhenian basin: Geophysical constraints on the nature of the main crustal domains. Journal of Geophysical Research: Solid Earth, 119(1):52–70. doi: 10.1002/2013JB010527. Copyright John Wiley & Sons, Inc. All rights reserved. Please visit: **https://agupubs.onlinelibrary.wiley.com/doi/full/10.1002/2013JB010527**. This figure is not included under the Creative Commons CC-BY 4.0 license of this publication) and (B) GH. Smt = seamount, R = ridge. C. Bathymetric and topographic map of the central Tyrrhenian Sea with the interpretation of the spatial distribution of the main basement domains (B and C are reproduced from Prada et al., 2015. The complex 3-D transition from continental crust to backarc magmatism and exhumed mantle in the Central Tyrrhenian basin. Geophysical Journal International, 203(1):63–78. doi: 10.1093/gji/ggv271. By permission of The Licensor through PLSclear. Copyright 2015, Oxford University Press. Please visit: **https://academic.oup.com/gji/article/203/1/63/577566**. This figure is not included under the Creative Commons CC-BY 4.0 license of this publication. For permissions, please visit: **https://plsclear.com/pages/ClearWizard.aspx**). D. Tectonic map of the Cornaglia-Magnaghi-Vavilov-Campania region showing the location of faults active during the Messinian and Early Middle Pliocene (Loreto et al., 2021). E. The three stages of formation of the Magnaghi-Vavilov Basin inferred from radiometric ages and stratigraphic information (Reproduced from Prada et al., 2016. Mantle exhumation and sequence of magmatic events in the Magnaghi–Vavilov Basin (Central Tyrrhenian, Italy): New constraints from geological and geophysical observations. Tectonophysics, 689:133–142. doi: 10.1016/j.tecto.2016.01.041. Copyright 2016, Elsevier B.V. All rights reserved. Please visit: **https://www.sciencedirect.com/science/article/pii/S0040195116000822?via%3Dihub**. This figure is not included under the Creative Commons CC-BY 4.0 license of this publication).

In the Vavilov Basin, a 30 m section of partially serpentinized peridotite under altered peridotite clasts and sediment sandwiched between two layers of basalt and basalt breccia was recovered at Site 651 (Figure **F2**) (Bonatti et al., 1990; Kastens and Mascle, 1990). MEDOC and CHIANTI $V_P$ models suggest that the Site 651 peridotite is not a local anomaly in an overall basaltic crust but that it rather represents an extended occurrence of exhumed mantle in the Vavilov and Magnaghi Basins (Figures **F4A–F4C**, **F5**). The CHIANTI cruise has found evidence of mantle exhumation also in the Marsili Basin, shown by high shallow velocities similarly to Magnaghi and Vavilov Basins, and a lack of PmP Moho reflections; Pliocene mantle exhumation in the Vavilov Basin (Figure **F4E**) was fast and coeval to or followed soon after by MORB volcanism (observed at Sites 655 and in the bottom basaltic unit of Site 651). Later, extension stopped or dramatically slowed down during the growth of the several kilometers tall Vavilov Seamount of calc-alkaline affinity, possibly corresponding to the shallow basaltic unit of Site 651. This sequence of events, where continental breakup and oceanic spreading is followed by mantle exhumation, differs from conventional models of lithospheric extension in COTs.

## 3.2. Seismic studies/site survey data

The supporting site survey data for Expedition 402 are archived at the IODP Site Survey Data Bank (SSDB) (**https://ssdb.iodp.org/SSDBquery/SSDBquery.php**; select 927 for proposal number).

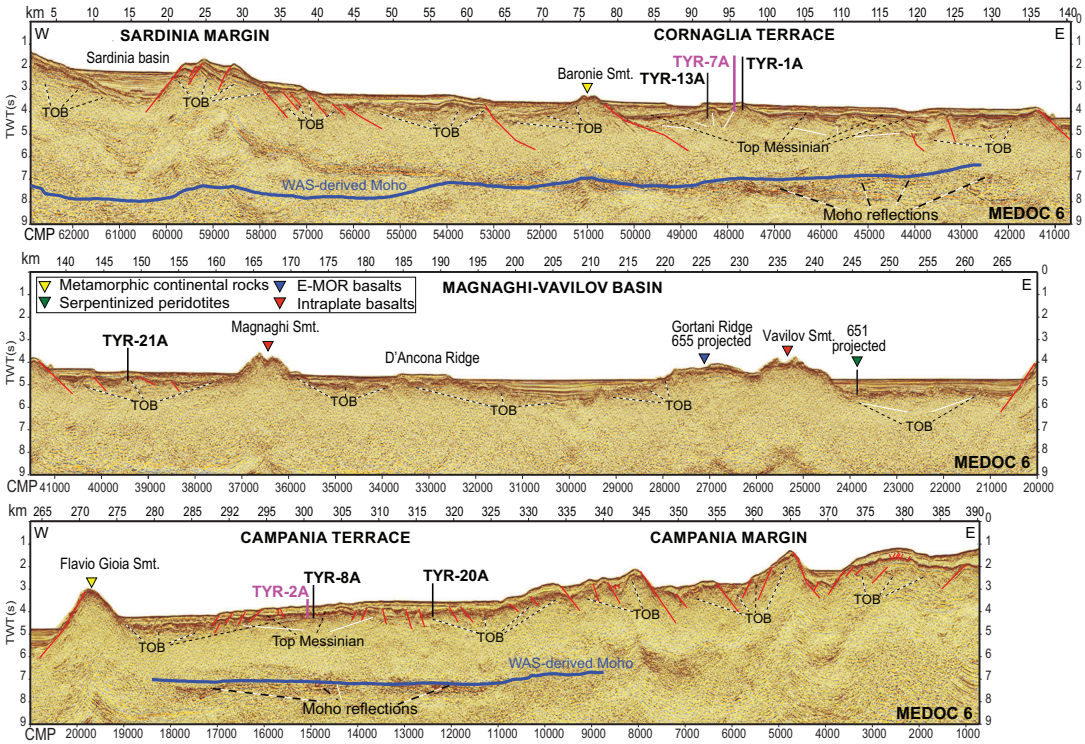


**Figure F5.** Time-migrated MCS profile MEDOC 6 (Prada et al., 2014) showing a consistent lack of Moho reflections beneath the Vavilov and Magnaghi Basins compared to the Moho inferred from WAS data (see also Figure F4B). In these profiles, Moho reflections (dashed black lines) terminate abruptly at the location where WAS-derived reflections also stop. TWT = two-way traveltime, CMP = common midpoint, TOB = top of basement, Smt = seamount. Reproduced from Prada et al., 2014. Seismic structure of the Central Tyrrhenian basin: Geophysical constraints on the nature of the main crustal domains. Journal of Geophysical Research: Solid Earth, 119(1):52–70. doi: 10.1002/2013JB010527. Copyright John Wiley & Sons, Inc. All rights reserved. Please visit: **https://agupubs.onlinelibrary.wiley.com/doi/full/10.1002/2013JB010527**. This figure is not included under the Creative Commons CC-BY 4.0 license of this publication.

# 4. Scientific objectives

Our main hypothesis is that the COT variability observed in the well-mapped Tyrrhenian basement was created by processes occurring at COTs worldwide. In particular, we interpret the sequence of events forming the Tyrrhenian COT to be related to vertical and/or horizontal mantle heterogeneities during the segmented opening of the basin. We propose that the 3-D variation observed in the Tyrrhenian Basin is typical of COT formation processes rather than the 2-D amagmatic mantle exhumation inferred from comparatively lower resolution studies.

The hypothesis, challenging current conventional wisdom, will be tested by addressing five scientific objectives, only achievable by drilling the basement in several locations:

1. To determine the kinematics and geometry of the extensional deformation in space and time.
2. To determine the heterogeneity of the mantle source and establish the timing and origin of the associated magmatism.
3. To establish the rheology, deformation patterns, and timing of mantle exhumation.
4. To determine the fluid-rock interactions in the peridotite basement.
5. To test models of rifting and COT formation.

To achieve these scientific objectives, Expedition 402 will drill two main transects:

1. An east–west transect to determine the nature of the basement and define the timing and relationships of mantle deformation, melting, and magmatic events. These goals will be accomplished by drilling a transect of four proposed sites (TYR-7A, TYR-2A, TYR-9A, and TYR-10A) (Figures **F1**, **F5**, **F6**) located in the Cornaglia Terrace (one site), in the exhumed mantle domain (two sites), and in the Campania Terrace (one site).
2. A north–south transect to establish the mechanisms and kinematics of mantle exhumation. Mantle exhumation appears to follow the general southward increase in crustal extension, from a relatively small amount in the northernmost Vavilov Basin to an ~100 km wide unroofing at 40° N. The roughly north–south transect has four proposed sites (TYR-11A and TYR-12A, with TYR-9A and TYR-10A also in the west–east transect) (Figures **F1**, **F6**) to map the spatial extension of the peridotite body that appears continuous in the north–south direction (Figures **F4**, **F6**).

## 4.1. To determine the kinematics and geometry of the extensional deformation in space and time

Determining the age of the extensional processes is key to understanding the kinematics of deformation and to constraining numerical simulations that relate deformation and melting. To achieve a full understanding of the process it is important to determine the ages of faulting, mantle deformation, and melting.

The age of synrift strata helps to define the kinematics of extensional faulting and thus the opening of the basins. Although this is straightforward in principle, most COTs worldwide are in ultradeepwater environments and are covered by thick postrift sediments. This prevents detailed dating and indirect age estimates vary greatly for any one basin. In West Iberia, with DSDP and ODP drilling in the Deep Galicia margin and Iberia Abyssal Plain, limits on the total drill string length restrained drilling to shallow portions of basement highs, penetrating only the youngest synrift strata. The results provide a general idea of the age progression of faulting (e.g., Ranero and Pérez-Gussinyé, 2010), but total rift duration estimates range 5–25 My (Whitmarsh et al., 2001). Furthermore, those ages only refer to continental extension because alteration of the mantle exhumed in Mesozoic times prevents detailed study of the mechanisms and age of the deformation from radioisotopic dating. There is currently no observational data that accurately constrain the timing of faulting, mantle deformation, and melting of any basin. Expedition 402 will provide the first robust and integrated data set from an entire COT system.

ODP Leg 107 established the basic Tyrrhenian stratigraphy (Kastens and Mascle, 1990), providing the framework to interpret seismic images. The basin has several stratigraphic markers, including three Messinian salinity crisis sediment units (>5.33–5.96 Ma), a local top Messinian erosional

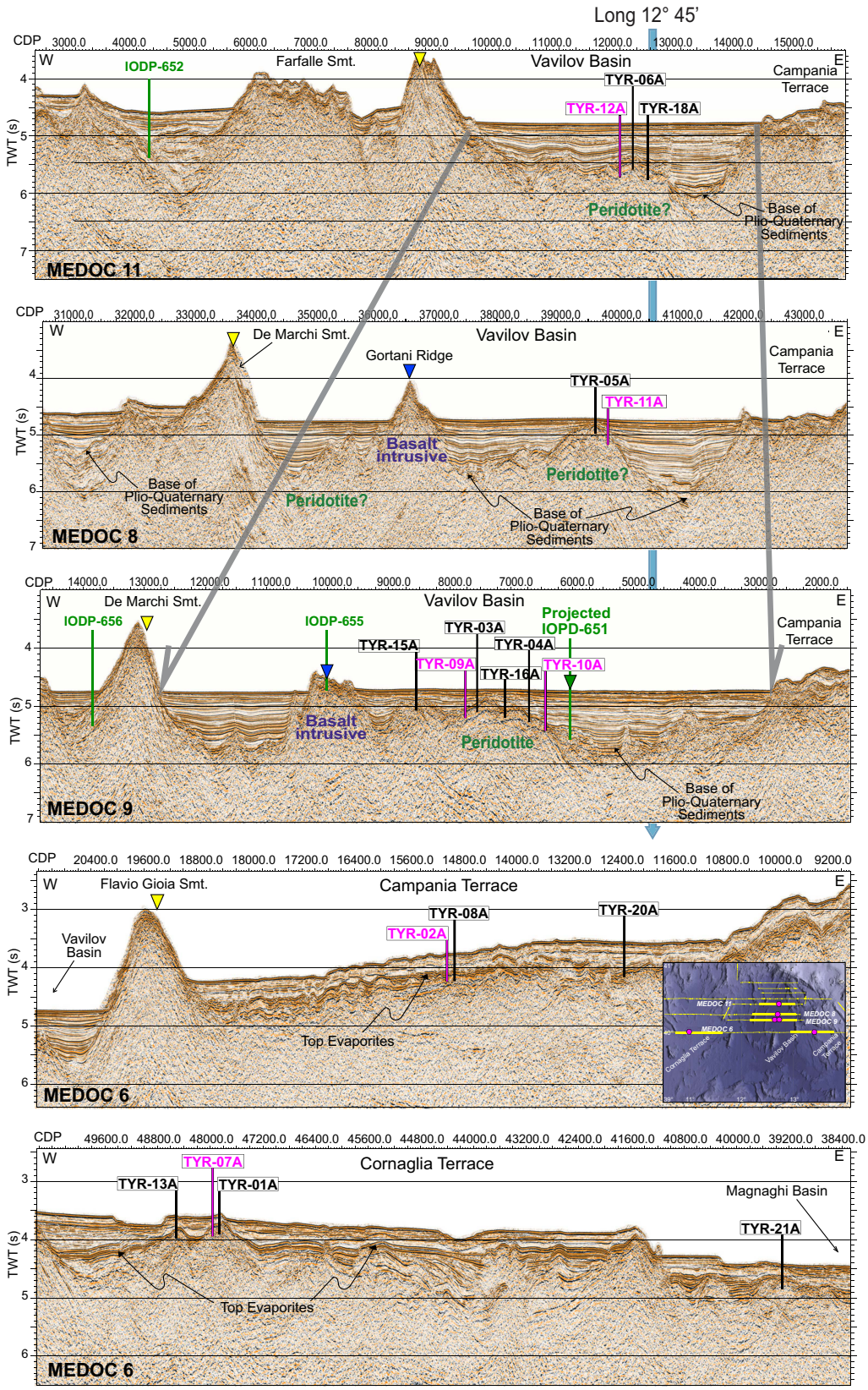


**Figure F6.** Close ups of the time-migrated MCS MEDOC Lines 6, 9, 8, and 11. Yellow triangle = metamorphic and granite rocks, blue triangle = E-MORB, green triangle = serpentinized peridotites. Primary drill site locations (pink) display target penetration depth. Alternate drill sites locations are shown in black. Inset: bathymetric map, produced using Emodnet data (EMODnet Bathymetry Consortium, 2018), with the location of WAS and MCS MEDOC transects. Yellow lines = location of seismic lines shown in this figure together with the drill site locations. TWT = two-way traveltime, CDP = common depth point, Smt = seamount.

unconformity (5.33 Ma), and a lower Pliocene intra-Zanclean unconformity (between 5.33 and 3.60 Ma). These markers provide excellent constraints on the timing of the opening of the basin.

However, existing stratigraphy constrains the opening of the continental crust but not the rates of mantle exhumation, which occurred during the Pliocene where available stratigraphic control is limited. Expedition 402 will refine the Pliocene stratigraphy by dating the sediment column, particularly with a detailed analysis of the oldest sediments on top of the basement. We will calibrate strata resting on the fault planes that exhumed mantle to determine, in time and space, the slip rate of the large domal faults that are seen in seismic images and resemble core complexes.

Age dating of sediment above basement will be achieved using calcareous nannofossils, which provide reliable biostratigraphy and biochronology in the Miocene–Pleistocene interval. The biozone resolution ranges 0.15–2.2 My in the interval 7.4–2.4 Ma and ~0.52 My in the interval 2.4–0 Ma. The analysis of nannofossils requires a small quantity of material and assemblages are generally very well preserved, resulting in a high-resolution biostratigraphy and precise dating. The age calibration will be much more accurate than at any other conjugate rift system. Chronology from biostratigraphy can be further calibrated by tephrochronology and magnetostratigraphy.

Dating fault activity will be crucial to understand the kinematics of mantle exhumation, the mechanisms of coeval peridotite deformation (Objective 3), and melt products (Objective 2, see below). Therefore, we will analyze lithospheric rheological evolution in time and space, a key to quantitatively understand the system.

Magmatic events will be dated with radioisotopes. Ar/Ar and K/Ar geochronology will be applied on lava glasses and basalt groundmasses, respectively. Leg 107 cores (Figure **F7**) contain many amphibole-bearing gabbroic patches and veins. These lithologies are excellent for dating and will help in defining the age of the gabbroic inclusions by K/Ar on amphiboles and feldspars and U/Th on zircon and xenotime.

## 4.2. To determine the heterogeneity of the mantle source and establish the timing and origin of the associated magmatism

A primary aim is to characterize the spatial and temporal variations of the mantle source through the coupled study of melting products and residual mantle. Structural, microstructural, petrologi-

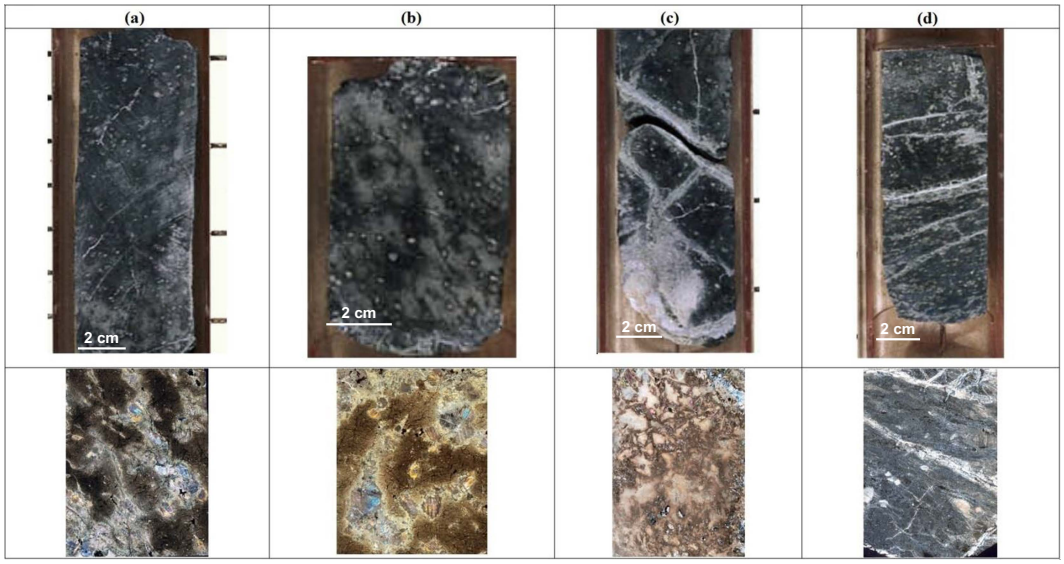


**Figure F7.** Top: Leg 107 Core 651A-58R illustrating different lithologies and structures of residual peridotites with variable degrees of late magmatic veining. Bottom: thin section micrograph of the same core (~2 cm wide). A. Dunite. B. Typical granular harzburgite. C. Highly depleted granular harzburgite with pervasive intrusion of late amphibole gabbroic veining heavily transformed to talc-chlorite and rodingite (651A-58R3, 20–37 cm). D. Centimeter-scale protomylonite harzburgite documenting high-temperature ductile strain localization in shear zones.

cal, geochemical, and geochronological studies of the exhumed mantle peridotites will establish the ductile mantle deformation, the mantle history of melting and melt extraction, melt retention and intrusion, and its 3-D variability. Exhumed mantle peridotites recovered at Site 651 (Figure **F2**) are spinel harzburgite and dunite with significant veining of amphibole gabbro. These peridotites record a protracted history of high-temperature ductile deformation, metasomatism, serpentinization, and brittle deformation (Bonatti et al., 1990). Our pilot microstructural study of Site 651 peridotites shows the existence of high-temperature (proto)granular harzburgite (Figure **F7A, F7B**), which is characteristic of asthenospheric flow and contains rare metasomatic/secondary clinopyroxene similarly to that observed in slow-spreading MOR environments (Brunelli et al., 2006; Seyler et al., 2007; Warren, 2016). Locally, the granular peridotites of Site 651 display pervasive amphibole-gabbro veins and patches (Figure **F7C**) (Bonatti et al., 1990) and are crosscut by relatively sharp shear bands expressed as protomylonitic domains (Figure **F7D**). Protomylonites are seldom observed in drilled abyssal peridotites from slow-spreading MORs (e.g., Jaroslow et al., 1996; Cipriani et al., 2009) but have been described in submersible surveys and sampling at the Iberian COT (Beslier et al., 1990). These protomylonites document retrograde nonmagmatic strain localization at high-deviatoric stress during mantle exhumation and suggest high-temperature shear zones extending into unaltered mantle rocks (Jaroslow et al., 1996).

Late synkinematic gabbroic veins (Figure **F7D**) indicate long-lived faulting and uplift from ductile deformation to brittle-plastic transition and further strain localization, coeval with melt impregnation and high-temperature hydrothermal activity. The latter feature is characteristic of detachment formation and evolution in mantle exhumed along oceanic core complexes in slow-spreading MORs (e.g., Escartín et al., 2017) and in magmatic COTs, both at slower spreading rates than the allegedly fast mantle exhumation in the Tyrrhenian Basin. Expedition 402 samples will be used for microstructural (combining electron backscattering diffraction [EBSD] in fresher samples) and geothermometry studies in pyroxene and spinel to reveal the mechanism of strain localization and the P-T-t cooling path, constraining the onset of mantle exhumation.

Analyses of bulk chemistry and geochemistry (major and trace elements and Re-Os isotopes), along with analyses of ortho/clinopyroxene couples for in situ major and trace elements and isotopes of Sr-Nd (and Hf-Pb in less depleted and refertilized peridotites) on mineral separates will provide information about the provenance, exhumation process, and lateral extent of mantle heterogeneities.

Site 651 peridotites are mostly devoid of clinopyroxene and have an extremely residual composition characterized by high Cr/Al in spinel and very low $Al_2O_3$ content (<1.0 wt%). This compositional character is markedly different from the subcontinental and oceanic mantle peridotites exposed in the circum-Tyrrhenian ophiolites and the Iberian COT, which are more fertile than the Tyrrhenian samples (Bonatti et al., 1990; Bodinier and Godard, 2007; Gonzalez-Jimenez et al., 2013). Site 651 mineral chemistry indicates high degrees of partial melting and melt extraction, with a composition similar to the most depleted peridotites found in slow-spreading to ultraslow-spreading MORs such as the Mid-Atlantic Ridge (MAR) and Gakkel Ridge (Warren, 2016) or those affected by fluid-flux melting in suprasubduction settings (Marchesi et al., 2006). It is unlikely that the residual character of the Site 651 peridotite is due to decompression partial melting leading to the early Tyrrhenian normal MORB (N-MORB) magmatic crust because such depletion in peridotite requires extremely high mantle potential temperatures and a long vertical decompression path (Herzberg, 2004). Also, fluid-flux melting would not explain the MOR composition of basaltic crust in the Tyrrhenian extended margins. Such depletion more likely sampled an unusually active convecting mantle, recording multiple episodes of (ancient) melting (Warren, 2016) or the presence of domains of old and buoyant Archean subcontinental mantle.

Our preliminary trace element chemistry of Site 651 peridotite minerals (Figure **F8A, F8B**) unveils a complex metasomatic and mantle melting history. Trace elements in granular peridotite orthopyroxenes (Figure **F9B**) show a highly heterogeneously distributed depleted mantle domains overprinted by late metasomatism events leading to enrichment in light rare earth elements (LREE) (Figure **F8B**). These data highlight the high potential of Expedition 402 core samples to unravel the melting and melt extraction history of the Tyrrhenian mantle through detailed trace element analyses of (relic) peridotite orthopyroxene, clinopyroxene, and olivine. We will also use Re-Os

analyses (whole rock and, if available, sulfides) to decipher the protracted history of past melting and to compare it to that of other circum-Mediterranean mantle peridotites (González-Jiménez et al., 2013). These data will not constrain the age of young melting events but they will decode their ancient melt-extraction history, which will be used to evaluate the potential role of inherited ancient mantle depletion (e.g., Harvey et al., 2006) as a potential factor controlling the switch from magmatic production to magma-poor mantle exhumation during COT formation.

Cenozoic igneous activity in the Tyrrhenian region is characterized by an extreme compositional variability in space and time, highlighting a complex evolutionary history for magmas and their sources. The Tyrrhenian Basin hosts Miocene to Quaternary volcanoes ranging in composition from MORB to BAB and ocean-island basalt (OIB). MORB-type rocks occur in the Vavilov Basin (Figure **F1**) and in other Tyrrhenian volcanoes. Rocks with an OIB fingerprint have been sampled at the Marsili, Vavilov, and Prometeo Seamounts and from Ustica Island (Trua et al., 2004, 2007; Peccerillo 2017). A melt inclusion study of the Marsili lavas (Trua et al., 2010) showed that the OIB component may derive from scattered blobs of African-type mantle instead of a well-developed asthenospheric flow as previously suggested (Trua et al., 2003). Defining the nature of different mantle components is a major goal of the project.

The first magmatic pulse precedes mantle exhumation and has been inferred from seismic velocities in the conjugate Cornaglia and Campania terraces, but it has not been sampled because it does not outcrop and was detected only recently (Prada et al., 2014, 2015, 2016). Expedition 402 sites will sample the volcanic layer associated with the first stages of magmatic spreading (Figures **F1**, **F5**, **F6**). Basalts recovered at Site 651 had fresh glassy rims, suggesting that newly drilled samples will provide enough glassy volcanic material for standard radioisotopic study (Sr-Nd-Hf-Pb) as well as high-precision Ar-Ar dating. These results will allow for investigating the temporal evolution of magmatism from normal mid-ocean ridge (N-MOR) to back-arc and OIB through the compositional evolution of basalts for major rare earth elements (REE), LILE, and HFSE and their source (Sr-Nd-Hf-Pb isotopes), constraining the temporal evolution of the melts involved in crustal accretion. Data from volcanic rocks will be compared with those of gabbroic inclusions in mantle peridotites to establish a potential link between mantle exhumation and volcanism.

Furthermore, we will establish the relationship between mantle source and Tyrrhenian volcanism. Our preliminary trace element investigation on a small sample set reveals a clear disequilibrium between the residual character of the rocks almost devoid of clinopyroxene and the extreme enrichment in incompatible elements in ortho- and clinopyroxenes (Figure **F8B, F8C**). LREE-enriched secondary clinopyroxenes at Site 651 peridotites (Figure **F8B**) are likely precipitated from the same melts that crystallized the amphibole-gabbroic impregnations in some peridotites (Figure **F8A**). These enriched patterns are rarely found in MOR and COT settings (Warren, 2016), but are present in Tyrrhenian OIB and arc-related volcanism (Figure **F9C, F9D**). Further characterization requires additional analyses of large clinopyroxenes in peridotite with variable depletion to reconstruct the primary composition of clinopyroxenes and reliably compute the trace element

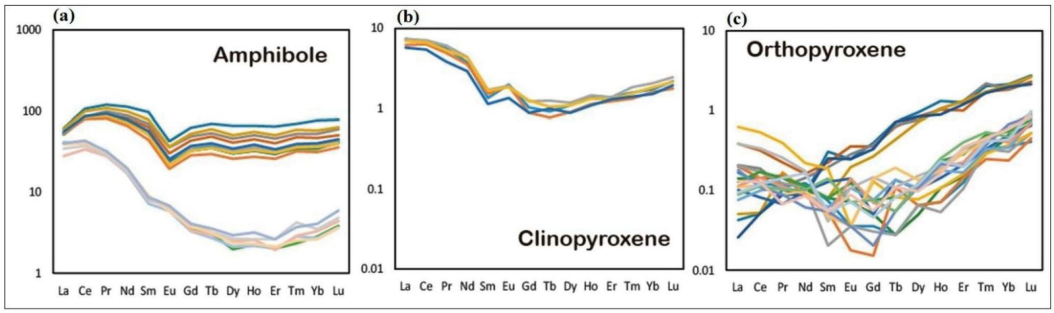


**Figure F8.** Chondrite-normalized extended trace element patterns from LA-ICP-MS analyses of minerals from peridotite and gabbroic rocks, Site 651 (unpublished preliminary results). A. Amphibole in gabbroic veins and patches (651A-58R3, 28–36 cm). B. Clinopyroxene in protogranular harzburgites (651A-58R1, 50–65 cm). C. Orthopyroxene (651A-58R1, 94–102 cm) in protogranular harzburgites.

composition of equilibrium melts (Figure F8). Constraining the source equilibrium melts will reveal the nature of lateral heterogeneities dispersed in the deep source and their genetic link with Tyrrhenian volcanism. For that, we will analyze trace element using laser ablation-inductively coupled plasma-mass spectrometry (LA-ICP-MS) and, if sufficient fresh material is recovered, Sr-Nd-Pb-Hf isotopes of mineral separates from gabbroic impregnations. Amphiboles from gabbroic veins and patches (Figure F8A) reveal different degrees of differentiation of the magmas involved, suggesting the presence of deep reservoirs or en route reactive differentiation. State-of-the-art high-precision U-Pb N-TIMS dating of zircon, xenotime and apatite in amphibole-gabbros patches will provide robust age constraints for mantle impregnation processes (e.g., Schärer et al.,

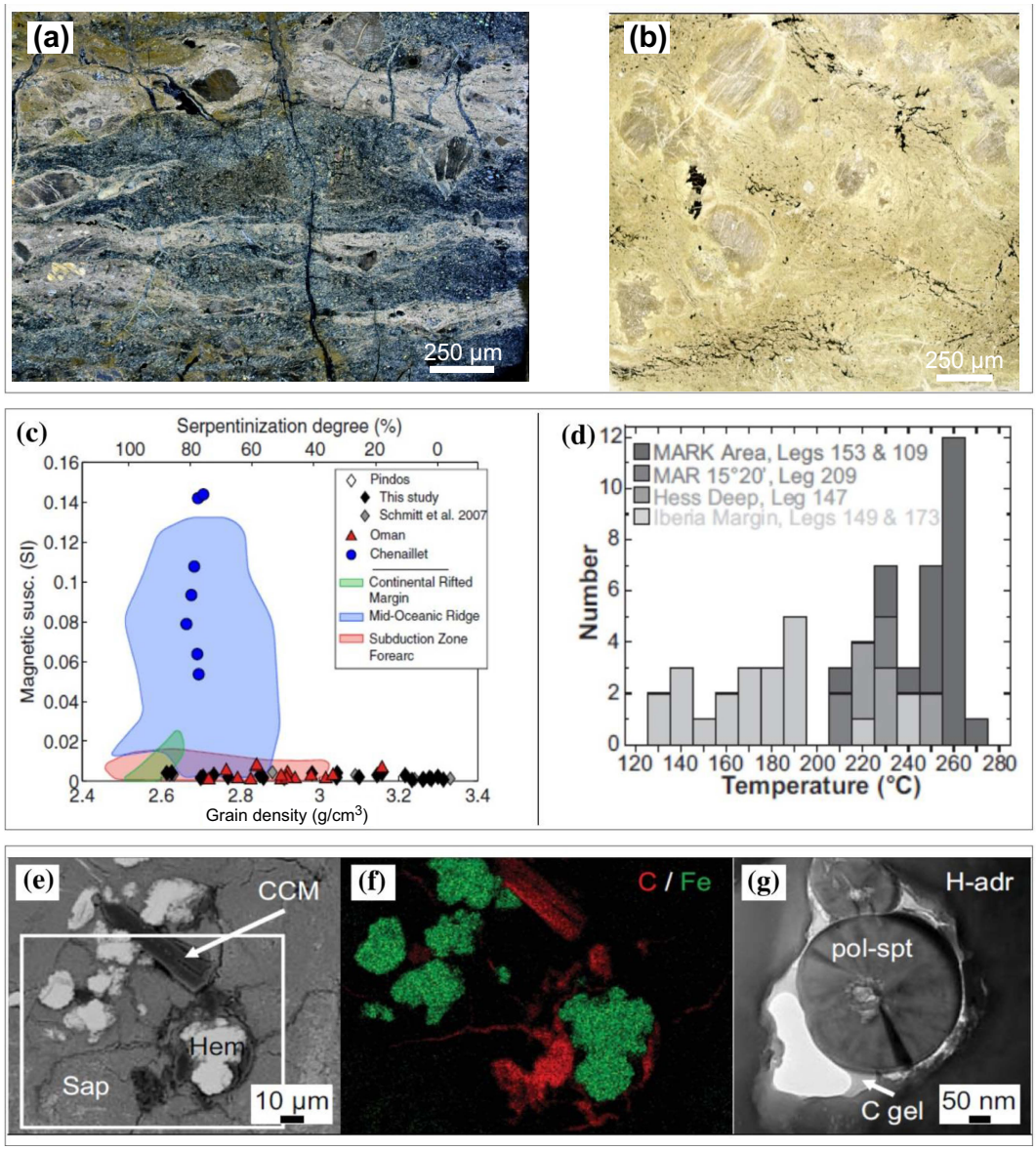


**Figure F9.** A. Deformation textures observed in cores from Hole 651A. B. Typical serpentinization textures of recovered peridotites. C. Compilation of existing data of magnetic susceptibility versus grain density in serpentinites. D. Histogram of serpentinization temperatures from oxygen isotope thermometry showing a bimodal distribution in magnetite-poor samples from the Iberia margin and magnetite-rich samples from MOR settings. E. O-bearing condensed abiotic carbonaceous matter (CCM) formed jointly with hematite (Hem) and saponite (Sap) during the low-temperature alteration (T < 150°C) of oceanic serpentinites. F. Associated elemental distributions of carbon and iron within the white square in E. G. Polyhedral serpentine (pol-spt) sections wet by a jelly film of organic carbon (C gel) interfacing between the pol-spt and the hydrogarnet (H-adr).

1995). A coupled Ar/Ar and K/Ar geochronology of the associated basalts will constrain the different magmatic phases.

## 4.3. To establish the rheology, deformation patterns and timing of mantle exhumation

Mantle exhumation in the Tyrrhenian recalls that occurring at slow- or ultraslow-spreading centers. In MOR contexts, exhumation is accommodated by two types of faulting:

1. Asymmetric detachment faulting associated with a nonnegligible amount of magmatism (accounting for ~50% of the extension) (Tucholke et al., 2007). This allows the formation under greenschist facies of a weak metasomatic talc-chlorite-amphibole assemblage that localizes deformation in a 100 m thick fault on top of a topographic high (e.g., MacLeod et al., 2002; Escartín et al., 2003, 2017).
2. Polarity change in a symmetric detachment fault system associated with a very limited magmatic supply (Sauter et al., 2013) and a poorly resolved deformation style, most probably localized in serpentinites.

The latter mechanism of exhumation is expected at COTs with poor magma supply, but it usually occurs at slower spreading rates than those estimated in the Tyrrhenian, where magmatic impregnation also documents nonnegligible magmatic activity (see Objective 2). By analogy with MOR systems (e.g., Cannat et al., 2008), the extensional style can vary with time depending on the evolution of the extension rate and magmatic supply in the Tyrrhenian Basin (see Objective 1).

The current limited sampling does not allow the identification of exhumation mechanisms and deformation modes in Tyrrhenian peridotites because no clear fault plane material was recovered. High-temperature fabrics in peridotites, shown by plastically deformed pyroxene, are the only deformation structures clearly described so far (Bonatti et al., 1990). However, the fabrics cannot account for the whole history of massive mantle exhumation to the surface, which implies lower temperature conditions. The available samples suggest that high-temperature deformation was actually localized in impregnated areas of peridotite samples, subsequently altered to talc-chlorite-amphibole, highlighting the role of magmatism in the early localization of deformation. Talc, having one of the lowest friction coefficients, is key in localizing deformation over a wide range of temperature conditions (Escartín et al., 2008). Such a weak assemblage, locally foliated, can reinforce the localization of deformation at low-temperature conditions (greenschist facies, also attested by broken pyroxene and amphiboles) and contribute to exhumation by faulting (Figure **F9A, F9B**). The capability of the tectonomagmatic interplay to create such an assemblage is similar to conditions in asymmetric detachment faults at MORs, but fault schists documenting high strain zones have not been collected yet.

Drilling peridotites at three sites in Expedition 402 will increase the likelihood to sample fault material from the principal slip surface and damage zone associated with the detachment. Detachment fault zones are ~75 m thick at MORs (Escartín et al., 2017), and secondary shear areas are locally observed down to 300 m into the footwall (Bonnemains et al., 2016). A fully silicified brecciated diabase occurs in the upper 70 m under a MOR detachment fault (Bonnemains et al., 2016). Drilling two sites to ~140 meters below seafloor (mbsf) into the Tyrrhenian peridotite will help understanding the deformation partitioning with depth, to be later used in numerical thermal models (Objective 5). MOR observations show that deformation mechanisms at exhumed mantle areas are heterogeneous and associated to variable intensity and type of hydrothermal processes. This highlights the complex interplay between hydrothermal fluid circulation, magmatism, and faulting and broadens the possible exhumation mechanisms and deformation modes in this setting, so that new Tyrrhenian samples may highlight unexpected processes.

## 4.4. To determine fluid-rock interactions in peridotite basement

Available peridotite samples from Leg 107 Sites 651 and 655 are largely hydrated, but some samples show pyroxene and olivine relics that can be used for magmatic studies (see Objective 2). Peridotites show different stages of alteration, ranging from amphibolite to greenschist facies, and also some low-temperature processes (<100°C) marked by clays and hydroxide formation (Bonatti

et al., 1990). Superficial alteration of peridotites by cold seawater during long-term exposure at the seafloor (i.e., leaching) can considerably modify the geochemical record of magmatic and hydrothermal processes but it is usually limited to the uppermost section. Static serpentinization is the dominant alteration process in peridotites (Figure **F9C, F9D**) away from melt impregnation; otherwise, the metasomatic assemblage talc-chlorite-amphibole is observed.

Serpentinization textures (mesh and bastite) are very similar to those observed at MORs, with abundant magnetite veins suggesting a formation temperature near 300°–350°C concomitant with exhumation tectonics (Bach et al., 2004; Andreani et al., 2007, 2013; Klein et al., 2014). From a geochemical point of view, serpentinites act as sponges for fluid mobile elements (Deschamps et al., 2011; Debret et al., 2013, 2014) and may have recorded a contribution from upward advected fluids, which has to be investigated. A comprehensive geochemical study will provide a unique data set to be compared with other settings (MORs, forearc, and subduction, e.g., Debret et al., 2018; Deschamps et al., 2013) and will address the details of water-rock exchanges in a COT. The search for fluid inclusions, direct markers of fluid circulating at depth, requires fresher samples such as those that will be recovered at the Expedition 402 sites.

A second stage of serpentinization forming serpentine textures poorer in magnetite is locally observed. Such textures are usually more abundant in ophiolites and continental rifted margins, where they are associated with very low magnetic susceptibilities and lower temperature of serpentinization (<150°–200°C) (Figure **F9E–F9G**) (Oufi and Cannat, 2002; Seyfried et al., 2007; Klein et al., 2014; Bonnemains et al., 2016). Extensive sampling for oxygen isotopes and magnetic measurements is required to test whether Tyrrhenian serpentinites differ from those at other COTs (Klein et al., 2014) where serpentinization temperature seems lower (Figure **F9G**).

The search for low-temperature (past or active) serpentinization or alteration in general in such systems is key to better constrain the seawater-lithosphere chemical exchange through time away from spreading centers after tectonomagmatic processes ceased. Although evidence of active serpentinization and/or alteration at temperature <200°C below inactive faults exists at MORs (e.g., Lost City at Atlantis massif, MAR; and Clamstone and Ghost City at Rainbow massif, MAR), its temporal extent has not been addressed by drilling because of the thick sediment cover away from the ridge. In particular, serpentinization is an unquantified contributor to $H_2$ production, carbon conversion and storage, and ecosystem development in oceanic lithosphere. $H_2$ and abiotic reduced carbon species, both volatile and condensed (see review in Andreani and Ménez, 2019), can be produced during serpentinization and sustain ecosystem development at shallow levels. Drilling Tyrrhenian peridotite provides the opportunity to quantify long-term alteration processes and test whether serpentinization is still active in the upper section of a peridotite that was exhumed at 2–5 Ma and is presently covered by sediment.

The Expedition 402 sites will allow for exploring the temperature and fluid composition with depth, and especially relate the distribution of $H_2$, organic volatiles, and ecosystems to rock properties. Different locations will address the lateral heterogeneity of possible outflow, complementing similar investigations of the recent IODP Expedition 357 at Atlantis Massif and the ICDP Oman Drilling project but in a different geological setting. Investigating redox-sensitive elements such as metals, S, and C will help to decipher the evolution of redox conditions and possible biogeochemical processes, especially at the basement/sediment interface where the strongest geochemical gradient are expected (e.g., Andreani et al., 2013; Debret et al., 2017, 2018; Ménez et al., 2018).

## 4.5. To test models of rifting and COT formation

Results from Objectives 1–4 will provide a unique data set, not available at other systems in the world, that will improve our understanding of the main parameters governing COT formation and that will allow for evaluating current COT formation models. The parameters, rather than the qualitative descriptions of models in literature, will provide the framework for model testing through quantitative numerical modeling.

Objectives 1–3 will provide the kinematics and geometry in space and time of the extensional deformation of the brittle layer and the transition from ductile to brittle deformation in the mantle as exhumation progressed.

The evolution in time and space of the deformation, integrated with an estimate of pressure and temperature conditions for mantle minerals and a melting evolutionary model resulting from Objectives 2 and 3 will provide the information needed to define the 3-D rheological evolution of the system.

The study of fluid-rock interactions in Objective 4, integrated with the information collected for Objectives 1–3, will help constrain the depth of penetration and strength of the hydrothermal system active during extension and after tectonism stopped. The model will be compared to predictions from the $V_P$ structure, obtained from seven WAS profiles with closely spaced ocean bottom seismometers as discussed above. The $V_P$ distribution was obtained with state-of-the-art travel time tomography and can be interpreted in terms of the distribution of porosity and rock type in basalts and of the degree of serpentinization in mantle peridotite. This information will further constrain the thermal and rheological structure of the extension system.

The holistic data set obtained in Expedition 402 will be used to constrain numerical models of lithospheric deformation, melt production, and mantle exhumation, reproducing the conditions of the Tyrrhenian system. The numerical code will be tested to investigate the range of parameter changes necessary to result in COT scenarios proposed in the literature and to evaluate the feasibility of reproducing them with physically realistic conditions.

Numerical models have shown that serpentinized mantle is exhumed at the COT when either the extension velocity is slow or the mantle was originally depleted (e.g., Pérez-Gussinyé et al. 2006; Ros et al., 2017). This applies particularly for strong rheologies. In contrast, weak lithospheric initial rheologies lead to ultrawide margins and no mantle exhumation but produce an abrupt transition to magmatic oceanic crust, as observed in the South China Sea (Ros et al., 2017; Davis and Lavier, 2017). Numerical models using constant mantle potential temperature and composition indicate that in cases where mantle exhumation and serpentinization occur first, melting progressively increases until a normal oceanic crust starts to form. In space, the continental crust is adjacent to the exhumed serpentinized mantle, and this is followed by magmatic oceanic spreading. The Tyrrhenian, however, challenges these results as here continental crust presents an abrupt transition to magmatic oceanic crust, followed by mantle exhumation. The data collected during Expedition 402 in combination with state-of-the-art numerical modeling will allow us to understand the conditions necessary to produce such an assemblage of basement domains and whether this might be common to rifted margins. MORs show significant lateral and temporal variations along and among ridge segments, from magmatic to nonmagmatic spreading. A similar change with time may lead to a structural configuration similar to that of the Tyrrhenian. Numerical models constrained by the data will allow mapping the parameters controlling these changes. Two potential candidates may be lateral mantle heterogeneities or changes in extension velocity.

State-of-the-art modeling techniques solve for the momentum, heat, and mass conservations equations of a visco-elasto-plastic lithosphere–asthenosphere system, allowing to simulate deformation, sedimentation, melting, serpentinization, and the dynamic interactions between these processes (Ros et al., 2017; Andrés-Martínez et al., 2019). These fully dynamic models can be adapted to simulate deformation in a cross section along a seismic profile, giving the location of brittle faults as inputs to the fully dynamic model. This will integrate kinematics with the evolution of temperature and rheology derived from Objectives 1–4 into detailed structural sections.

Numerical models will also incorporate hydrothermal circulation and the thermodynamics of fluid-rock interactions. The study of fluid-rock interactions of Objective 4, integrated with the information collected for Objectives 1–3, will provide strong constraints on the depth of penetration and strength of the hydrothermal system active during extension and after tectonism stopped. Thus the combination of modeling and observations will allow us to analyze the influence of fluids in the mode of deformation and also the role of fluid-rock interaction in element exchange.

Finally, the petrology predicted by numerical simulations will be transformed to $V_P$ and compared to the velocities estimated from the WAS data, and analyzed in light of the petrological drilling results.

### 4.6. Relationship with the Scientific Ocean Drilling 2050 Science Framework

The data collection and scientific activities of Expedition 402 will directly address a strategic objective and a flagship initiative defined in the comprehensive 2050 Science Framework. For the strategic objective of "the oceanic life cycle of tectonic plates," Expedition 402 will explore the early evolution of oceanic lithosphere following continental rifting in a favorable location with a thin sediment cover, including the initial stage of ocean crust formation, the variation of fundamental rifting modes (from magma-rich to magma-deprived), and the serpentinization of mantle rocks exhumed at COTs. For the flagship initiative "probing the deep Earth," Expedition 402 will complement efforts to characterize the oceanic lithosphere by providing samples and measurements of mantle rocks such as those exposed in oceanic core complexes at slow-spreading MORs and by investigating the fluid exchange in the subseafloor between sediments, oceanic crust, and mantle.

## 5. Operations plan and coring strategy

To accomplish the scientific objectives described above, Expedition 402 will reach the Tyrrhenian basement at six sites. Four proposed sites in the Vavilov Basin target exhumed mantle (TYR-9A, TYR-10A, TYR-11A, and TYR-12A) and proposed sites on the Cornaglia and Campania terraces (TYR-7A and TYR-2A) target magmatic basement. The site locations are arrayed in west–east and north–south transects, with Site TYR-9A at the center of the two transects (Figure **F1**). The primary drill sites, alternate sites, and drilling and coring strategies are described below (Figure **F10**; Tables **T1**, **T2**).

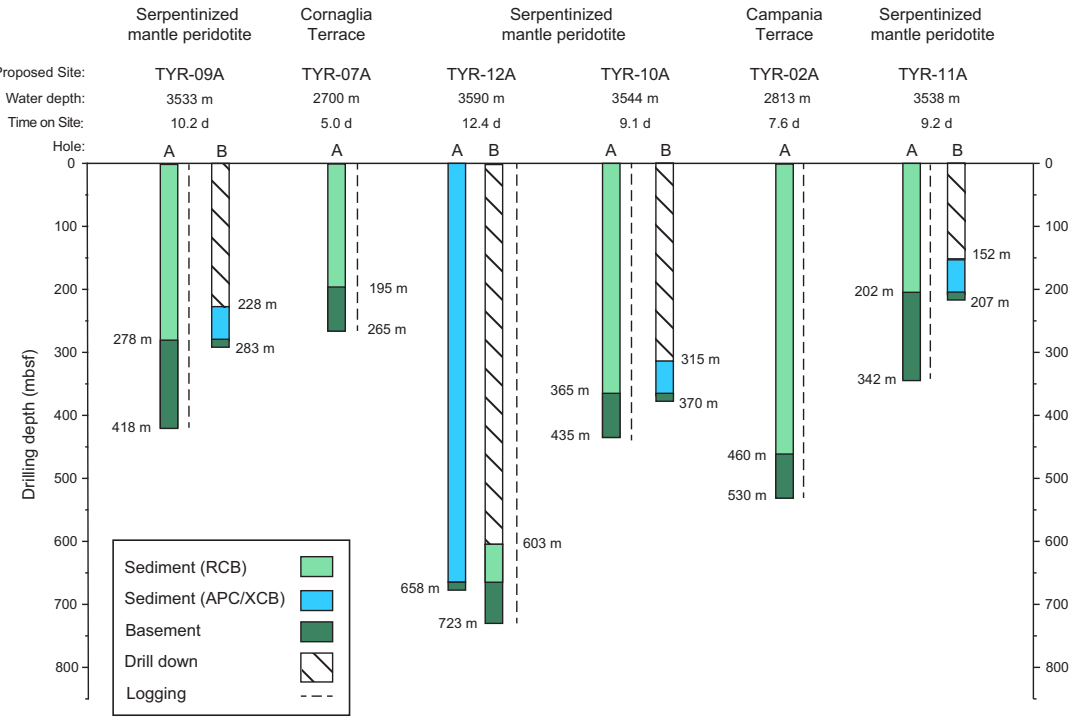


**Figure F10.** Coring operations strategy, including type of coring, target depth, and target lithology, for the six primary sites of Expedition 402.

**Table T1.** Coring strategy and time estimates for the six primary sites of Expedition 402. Maximum penetration depth approved by Environmental Protection and Safety Panel (EPSP) listed under each site number; at all sites, EPSP approved deepening of holes as time is available. mbrf = meters below rig floor, mbsf = meters below seafloor. RCB = rotary core barrel, APC = advanced piston corer, XCB = extended core barrel, SET2 = Sediment Temperature 2 tool, triple combo = triple combination tool string, FMS = Formation MicroScanner.

| Site No. | Location (Latitude Longitude) | Seafloor Depth (mbrf) | Operations Description | Transit (days) | Drilling Coring (days) | Logging (days) |
|---|---|---|---|---|---|---|
| Napoli | | | Begin Expedition 5.0 | port call days | | |
| | | | Transit ~87nmi toTYR-09A@ 10.5 | 0.3 | | |
| TYR-09A | 40° 11.0328' N | 3544 | Hole A - RCB 418 mbsf; 3 SET2; Log Triple Combo, FMS-Sonic | 0 | 7.1 | 1.2 |
| EPSP | 12° 37.9458' E | | Hole B - APC/XCB Drill 228 mbsf; XCB Core 283 mbsf | 0 | 1.9 | 0.0 |
| to 418 mbsf | | | | | | |
| | | | Sub-Total Days On-Site: 10.2 | | | |
| | | | Transit ~76nmi toTYR-07A@ 10.5 | 0.3 | | |
| TYR-07A | 40° 0.0582' N | 2711 | Hole A - RCB 265 mbsf; 3 SET2; Log Triple Combo, FMS-Sonic | 0 | 4.0 | 1.0 |
| EPSP | 10° 59.1732' E | | | | | |
| to 265 mbsf | | | | | | |
| | | | Sub-Total Days On-Site: 5.0 | | | |
| | | | Transit ~83nmi toTYR-12A@ 10.5 | 0.3 | | |
| TYR-12A | 40° 24.9540' N | 3601 | Hole A - APC/HLAPC 300 mbsf; XCB 658 mbsf | 0 | 6.1 | 0.0 |
| EPSP | 12° 42.4560' E | | Hole B - RCB Drill 603 mbsf; RCB 723 mbsf; 3 SET2; Log Triple Combo, FMS-Sonic | 0 | 4.8 | 1.4 |
| to 723 mbsf | | | | | | |
| | | | Sub-Total Days On-Site: 12.4 | | | |
| | | | Transit ~14nmi toTYR-10A@ 1.5 | 0.4 | | |
| TYR-10A | 40° 11.0388' N | 3555 | Hole A - RCB 435 mbsf; 3 SET2; Log Triple Combo, FMS-Sonic | 0 | 5.8 | 1.2 |
| EPSP | 12° 42.4956' E | | Hole B - APC/XCB Drill 315 mbsf; XCB 370 mbsf | 0 | 2.1 | 0.0 |
| to 435 mbsf | | | | | | |
| | | | Sub-Total Days On-Site: 9.1 | | | |
| | | | Transit ~34nmi toTYR-02A@ 10.5 | 0.1 | | |
| TYR-02A | 40° 0.0216' N | 2824 | Hole A - RCB 530 mbsf; 3 SET2; Log Triple Combo, FMS-Sonic | 0 | 6.4 | 1.2 |
| EPSP | 13° 24.4670' E | | | | | |
| to 632 mbsf | | | | | | |
| | | | Sub-Total Days On-Site: 7.6 | | | |
| | | | Transit ~36nmi toTYR-11A@ 10.5 | 0.1 | | |
| TYR-11A | 40° 15.9684' N | 3549 | Hole A - RCB 342 mbsf; 3 SET2; Log Triple Combo, FMS-Sonic | 0 | 6.3 | 1.1 |
| EPSP | 12° 42.3174' E | | Hole B - APC/XCB Drill 152 mbsf; XCB to 207 mbsf | 0 | 1.8 | 0.0 |
| to 342 mbsf | | | | | | |
| | | | Sub-Total Days On-Site: 9.2 | | | |
| | | | Transit ~82nmi toNapoli@ 10.5 | 0.3 | | |
| Napoli | | | End Expedition | 2.0 | 46.3 | 7.1 |

| | | | |
|---|---|---|---|
| Port Call: | 5.0 | Total Operating Days: | 55.4 |
| Sub-Total On-Site: | 53.4 | Total Expedition: | 60.4 |

**Table T2.** Coring strategy and time estimates for Expedition 402 alternate sites. Maximum penetration depth approved by Environmental Protection and Safety Panel (EPSP) listed under each site number; at all sites, EPSP approved deepening of holes as time is available. mbrf = meters below rig floor, mbsf = meters below seafloor, LWD = logging while drilling, MWD = measurement while drilling. RCB = rotary core barrel, APC = advanced piston corer, HLAPC = half-length APC, XCB = extended core barrel. SET2 = Sediment Temperature 2 tool, triple combo = triple combination tool string, FMS = Formation MicroScanner.

| Site No. | Location (Latitude Longitude) | Seafloor Depth (mbrf) | Operations Description | Drilling Coring (days) | LWD/MWD Log (days) |
|---|---|---|---|---|---|
| TYR-01A | 40.000850° N | 2686 | Hole A - RCB 234 mbsf; 3 SET2; Log Triple Combo, FMS-Sonic | 2.2 | 0.9 |
| EPSP | 10.994272° E | | | | |
| to 234 mbsf | | | | | |
| | | | Sub-Total Days On-Site: 3.1 | | |
| TYR-03A | 40.183880° N | 3544 | Hole A - RCB 360 mbsf; 3 SET2; Log Triple Combo, FMS-Sonic | 3.6 | 1 |
| EPSP | 12.641300° E | | Hole B - APC/XCB Drill 170 mbsf; XCB 225 mbsf | 1.6 | 0 |
| to 360 mbsf | | | | | |
| | | | Sub-Total Days On-Site: 6.3 | | |
| TYR-04A | 40.184020° N | 3557 | Hole A - RCB 548 mbsf; 3 SET2; Log Triple Combo, FMS-Sonic | 5.4 | 1.2 |
| EPSP | 12.728010° E | | Hole B - APC/XCB Drill 428 mbsf; XCB 483 mbsf | 2.3 | 0 |
| to 438 mbsf | | | | | |
| | | | Sub-Total Days On-Site: 8.9 | | |
| TYR-05A | 40.266090° N | 3541 | Hole A - RCB to 228 mbsf, 3 SET2; Log Triple Combo, FMS-Sonic | 3.8 | 0.9 |
| EPSP | 12.694320° E | | Hole B - APC/XCB 93 mbsf | 1.2 | 0 |
| to 228 mbsf | | | | | |
| | | | Sub-Total Days On-Site: 5.9 | | |
| TYR-08A | 40.000360° N | 2848 | Hole A - RCB 524 mbsf; 3 SET2; Log Triple Combo, FMS-Sonic | 4.9 | 1.1 |
| EPSP | 13.385832° E | | | | |
| to 752 mbsf | | | | | |
| | | | Sub-Total Days On-Site: 6.1 | | |
| TYR-13B | 40.001003° N | 2724 | Hole A - RCB 380 mbsf; 3 SET2; Log Triple Combo, FMS-Sonic | 4.9 | 1 |
| EPSP | 10.955490° E | | | | |
| to 1277 mbsf | | | | | |
| | | | Sub-Total Days On-Site: 5.9 | | |
| TYR-14A | 39.712730° N | 3392 | Hole A - RCB 566 mbsf; 3 SET2; Log Triple Combo, FMS-Sonic | 6.9 | 1.2 |
| EPSP | 13.315000° E | | | | |
| to 566 mbsf | | | | | |
| | | | Sub-Total Days On-Site: 8.1 | | |
| TYR-15A | 40.184200° N | 3611 | Hole A - RCB 315 mbsf; 3 SET2; Log Triple Combo, FMS-Sonic | 6.3 | 1 |
| EPSP | 12.567100° E | | Hole B - APC/XCB Drill 125 mbsf; XCB 180 mbsf | 1.9 | 0 |
| to 291 mbsf | | | | | |
| | | | Sub-Total Days On-Site: 9.2 | | |
| TYR-16A | 40.183870° N | 3589 | Hole A - RCB 341 mbsf; 3 SET2; Log Triple Combo, FMS-Sonic | 5.1 | 1 |
| EPSP | 12.677170° E | | Hole B - APC/XCB Drill 221 mbsf; XCB 276 mbsf | 2.3 | 0 |
| to 341 mbsf | | | | | |
| | | | Sub-Total Days On-Site: 8.4 | | |
| TYR-17A | 40.331210° N | 3611 | Hole A - RCB 602 mbsf; 3 SET2; Log Triple Combo, FMS-Sonic | 8.8 | 1.3 |
| EPSP | 12.673040° E | | Hole B - APC/XCB Drill 412 mbsf; XCB 467 mbsf | 3.5 | 0 |
| to 602 mbsf | | | | | |
| | | | Sub-Total Days On-Site: 13.5 | | |
| TYR-18A | 40.416000° N | 3611 | Hole A - APC/HLAPC 300 mbsf; 4X APCT3; XCB 626 mbsf | 6.3 | 0 |
| EPSP | 12.744240° E | | Hole B - RCB Drill 571 mbsf; 3 SET2; RCB 691 mbsf; Log Triple Combo, FMS-Sonic | 4.6 | 1.3 |
| to 691 mbsf | | | | | |
| | | | Sub-Total Days On-Site: 12.2 | | |
| TYR-19A | 40.385620° N | 3612 | Hole A - APC/HLAPC 300 mbsf; 4X APCT3; XCB 1068 msbf | 11.1 | 0 |
| EPSP | 12.744280° E | | Hole B - RCB Drill 1013 mbsf; 3 SET2; RCB 1133 mbsf; Log Triple Combo, FMS-Sonic | 5.7 | 1.7 |
| to 1133 mbsf | | | | | |
| | | | Sub-Total Days On-Site: 18.5 | | |
| TYR-20A | 39.999778° N | 2709 | Hole A - RCB 470 mbsf; 3 SET2; Log Triple Combo, FMS-Sonic | 5.3 | 1.1 |
| EPSP | 13.595834° E | | | | |
| to 470 mbsf | | | | | |
| | | | Sub-Total Days On-Site: 6.3 | | |
| TYR-21A | 40.001163° N | 3377 | Hole A - RCB 409 mbsf; 3 SET2; Log Triple Combo, FMS-Sonic | 6.7 | 1 |
| EPSP | 11.625110° E | | Hole B - APC/XCB Drill 219 mbsf; XCB 274 mbsf | 2.1 | 0 |
| to 339 mbsf | | | | | |
| | | | Sub-Total Days On-Site: 9.8 | | |

Prioritization of the primary sites is: TYR-9A, TYR-7A, TYR-12A, TYR-10A, TYR-11A, and TYR-2A. Coring at Site TYR-9A aims to recover mantle peridotites of the Vavilov Basin; it is one of the two sites where we plan a deep penetration of 140 m into basement. Site TYR-7A is located on the Cornaglia Terrace, along the west–east transect, and targets the preexhumation basalts. Site TYR-12A targets the upper mantle peridotites in the northernmost portion of the Vavilov Basin. It belongs to the north–south transect and will core the sedimentary succession (~650 m) of this basin using the advanced piston corer (APC)/extended core barrel (XCB) system. Coring at Sites TYR-10A and TYR-11A will also target mantle peridotites and will complete the north–south transect, and Site TYR-2A targets preexhumation basalts on the Campania Terrace and completes the west–east transect. Site TYR-2A is lower priority than Site TYR-11A; however, Site TYR-2A will be drilled first so that any remaining expedition time can be used deepening the basement hole at Site TYR-11A beyond 140 m subbasement (Figure **F10**; Table **T1**). Basement holes at all sites may also be deepened as time allows.

A goal for at least two sites that target the mantle peridotites is to core and log across the exhumation fault zone, assumed to be approximately ≤100 m thick (Escartín et al., 2017). To meet this objective, Sites TYR-09A and TYR-11A will penetrate 140 m into the mantle (accounting also for a standard logging tool string length of ~35 m), and Sites TYR-12A and TYR-10A will penetrate 70 m, which might be enough to drill through the fault as well (Figure **F10**; Table **T1**). Sites TYR-07A and TYR-02A in the Cornaglia and Campania Terraces, respectively, will penetrate 70 m into basement basalt (Figure **F10**; Table **T1**).

The coring strategy at all sites except TYR-12A is to first core and log Hole A to the target depth using the rotary core barrel (RCB) system (Figure **F10**; Tables **T1**, **T2**). Core recovery is particularly important in the few tens of meters above basement to calibrate ages based on microfossils and to evaluate rock-fluid interactions and possible biogeochemical evidence of active serpentinization at depth. As such, if core recovery or quality in Hole A is deemed insufficient in this critical interval, the plan is to drill an additional Hole B down to ~50 m above the base of the sediment column and continue coring to the top of basement with the APC/XCB coring system. Site TYR-12A should recover a complete sediment section, and the plan at this site is to core first by APC/XCB a Hole A to the basement and then core by RCB and log a Hole B that samples ~70 m of basement rocks. Pore water samples will be taken in at least one hole per site to study fluid-rock interactions and microbial communities.

## 5.1. Proposed drill sites

### 5.1.1. Exhumed mantle peridotites in the Vavilov Basin

Primary Sites TYR-9A, TYR-10A, TYR-11A, and TYR-12A are in the Vavilov Basin (Figure **F1**) and target exhumed mantle peridotites. At each of these sites, the general operations plan is to RCB core with recovery through the sedimentary section, capture the sediment/basement interface, and then continue RCB coring either 70 m (Sites TYR-10A and TYR-12A) or 140 m (Sites TYR-9A and TYR-11A) into basement. This plan ensures that at least two sites cross the exhumation fault zone, assumed to be ~100 m thick or less (Escartín et al., 2017). Three or four temperature measurements will be collected at each site using the Sediment Temperature 2 (SET2) tool with the RCB coring system. RCB holes recovering mantle peridotites will be logged following RCB coring using the triple combination (triple combo) and Formation MicroScanner (FMS)-sonic tool strings. The Ultrasonic Borehole Imager (UBI) tool string may be deployed in addition to or replacing the FMS, as time, hole conditions, and tool availability allow. If recovery across the sediment/basement interface is low or poor quality in Hole A using the RCB system, a second hole will be cored using the APC/XCB system to recapture the interface. In this second hole, we will drill down using the APC/XCB system to 50 m above basement and then begin XCB coring, recovering the 50 m of sediment overlying basement and up to 5 m of basement. Recovery is particularly important in the tens of meters above the basement to calibrate ages on microfossils and to evaluate rock-fluid interaction for possible biogeochemical evidence of active serpentinization at depth.

Site TYR-9A (alternates: Sites TYR-3A, TYR-15A, and TYR-21A) is considered the highest priority site because of its location near the intersection of the planned west–east and north–south transects across the basin and, as such, will be the first site visited during Expedition 402 (Figures **F11**, **F12**). The water depth at Site TYR-9A is 3533 m. In Hole A, we plan to RCB core to a total depth of 418 mbsf, including an expected 278 m of sediment and 140 m of basement. This depth of basement penetration will theoretically cross the exhumation fault zone at ~100 m or less below the top of basement (Escartín et al., 2017). As time allows, and if recovery of the sediment/basement interface in Hole A was poor, a second hole will drill down to 228 mbsf using the APC/XCB coring system, followed by coring the lowermost 50 m of sediment to reach the sediment/basement interface. Alternate Sites TYR-3A and TYR-15A are adjacent to Site TYR-9A along the same seismic line (Figure **F11**), whereas alternate Site TYR-21A is in the Magnaghi Basin, 48 nmi distance away from Site TYR-09A, but with similar water depth and sediment cover (Figure **F12**). Alternate sites will be drilled with the same strategy. Site TYR-3A is located at 3533 mbsf, and RCB coring is planned to 360 mbsf (220 m sediments plus 140 m serpentinized peridotites). Site TYR-15A is located at 3600 mbsf, and RCB coring is planned to 315 mbsf (175 m sediments plus 140 m serpentinized peridotites). Site TYR-21A is located at 3366 mbsf, and RCB coring is planned to 409 mbsf (269 m sediments plus 140 m serpentinized peridotites).

**Site Figure** **IODP proposal P927** **Site TYR-09A**

| | |
|---|---|
| Priority: | Primary |
| Position: | 40,18388 ° N; 12,63243 ° E<br>Abyssal plan of Vavilov Basin |
| Water depth (m): | 3533 |
| Target drilling depth (mbsf): | 418 |
| Approved maximum penetration (mbsf): | Discretion of shipboard party to deepen the hole if time is available |
| Survey coverage (track map; seismic profile): | Medoc9_2200-11000.sgy (CDP 7720) |
| Objective(s): | Recovery of serpentinized peridotite underneath Plio-Quaternary sediments |
| Coringprogram: | Hole A: RCB to total depth<br>Hole B: APC/XCB from the deepest 50 m of sediments plus 5 m into the basement |
| Downhole measurements program: | Hole A: Wireline log with triple combo, FMSsonic |
| Nature of rock anticipated: | 278 m of terrigenous sand/silt/clay followed by 140 m of serpentinized peridotites |

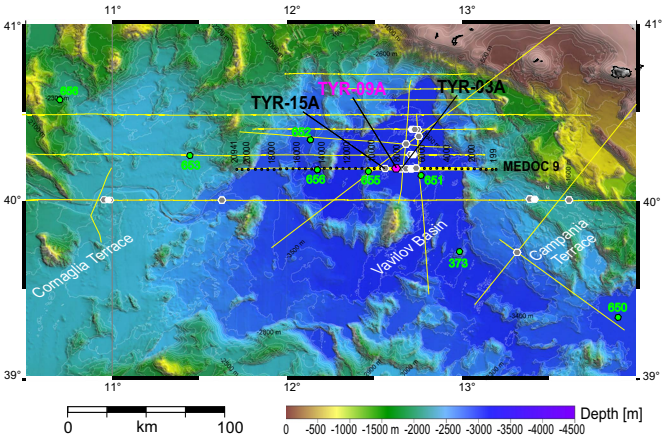


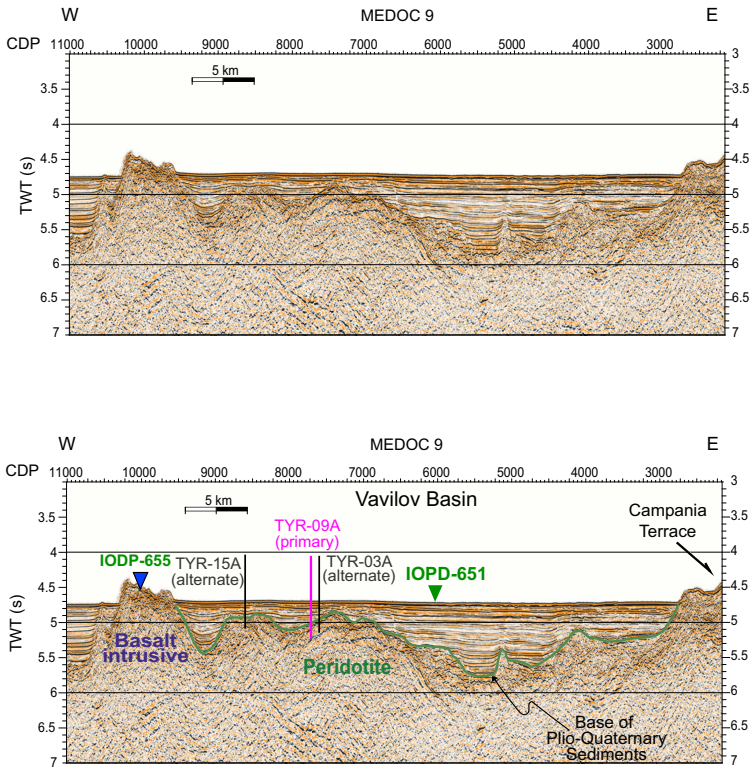


**Figure F11.** Location and seismic lines for Site TYR-09A and its alternates, TYR-03A and TYR-15A. Bottom seismic line panel: interpreted sediment-basement interface, site locations, and approximate planned penetration are shown. The drilling target is the rocks located below the base of the Pliocene–Quaternary sediments (green line). Locations of Sites 651 and 655 are also noted. CDP = common depth point, TWT = two-way traveltime.

After completing the intersection of the two transects at Site TYR-9A, we will core at Site TYR-7A on the Cornaglia Terrace (strategy described in the next section) and then return to the Vavilov Basin to core Site TYR-12A, the northernmost site along the north–south transect. Site TYR-12A has a water depth of 3590 m, with 653 m of sediment overlying basement (Figure **F13**). This site has the thickest sediment cover of all planned sites; as such, we plan to recover the complete succession with the APC/XCB system in Hole A, including recovery of the sediment/basement interface. The target of this site are the upper mantle peridotites, so a second hole will drill ahead with the RCB system to 603 mbsf, recapture the lower 50 m of sediment and sediment/basement interface, including three temperature measurements with the SET2 tool, and then core 70 m of basement. This second hole will then be logged with the triple combo and FMS-sonic tool strings. As at the other sites, recovery of the interface is important for dating and for investigation of serpentinization reactions at depth. This selected depth of basement penetration may cross the exhumation fault zone, but balances coring time with priority operations at other sites. Sites TYR-18A and TYR-19A are alternates for primary Site TYR-12A (Figures **F13**, **F14**). Alternate Site TYR-06A was not approved for operations. Site 18A is along the same seismic line as Site TYR-12A, and Site TYR-19A is at the intersection of MCS Lines ST-03 and M29B. The drilling strategy is unchanged. Both sites are at a water depth of ~3600 m. The complete sedimentary succession will be sampled with the APC/XCB tool in Hole A to 626 mbsf (621 m sediments plus 5 m

**Site Figure** **IODP proposal P927** **Site TYR-21A**

| | |
|---|---|
| Priority: | Alternate of TYR-09A |
| Position: | 40.00116° N; 11.62511° E<br>Magnaghi Basin |
| Water depth (m): | 3366 |
| Target drilling depth (mbsf): | 409 |
| Approved maximum penetration (mbsf): | Discretion of shipboard party to deepenthe hole if time is available |
| Survey coverage (track map; seismic profile): | Medoc6_TYR21A_CDP36250-41950.sgy<br>(CDP 39250) |
| Objective(s): | Recovery of basalts underneath<br>Plio-Quaternary sediments deposits |
| Coring program: | Hole A: RCB to total depth<br>Hole B: APC/XCB from the deepest 50 m<br>of sediments plus 5 m into the basement |
| Downhole measurements program: | Hole A: Wireline log with triple combo, FMS-sonic |
| Nature of rock anticipated: | 269 m of terrigenous sand/silt/clay,<br>plus 140 m of serpentinized mantle peridotites |

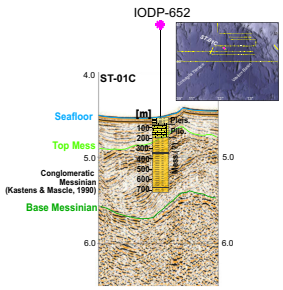


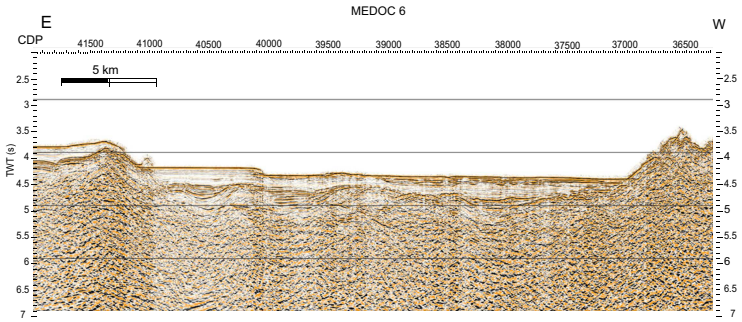


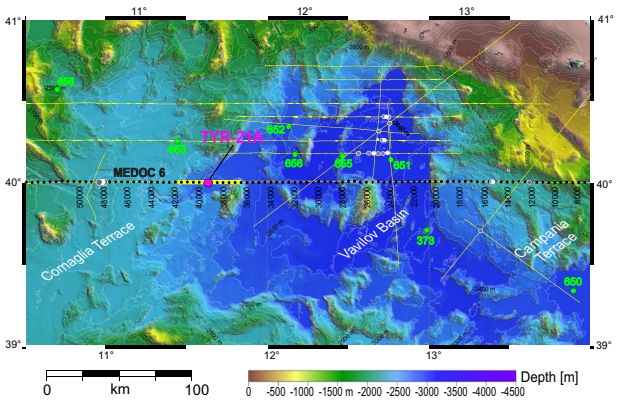


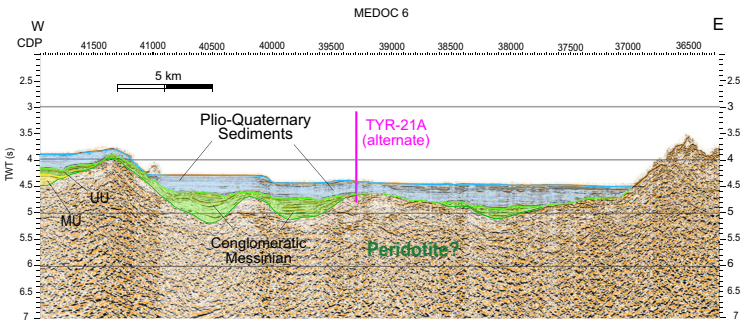


**Figure F12.** Site TYR-21A (alternate of TYR-09A). Bottom seismic line panel: interpreted sediment-basement interface, site location, and approximate planned penetration are shown. The drilling target is the rocks located below the base of the Pliocene–Quaternary sediments (green line). CDP = common depth point, TWT = two-way traveltime, MU = mobile unit, UU = upper unit.

serpentinized peridotites) and then Hole B will drill down to 571 m followed by RCB to 691 m (50 m sediments plus 70 m serpentinized peridotite). For Site TYR-19A, which has a much thicker sediment coverage, we will core with the APC/XCB in Hole A to 1068 mbsf (1063 m sediments plus 5 m serpentinized peridotites), Hole B drill down to 1013 m followed by RCB to 1133 m (50 m sediments plus 70 m serpentinized peridotite).

Site TYR-10A and its alternate Sites TYR-4A and TYR-16A are within the Vavilov Basin along the west–east transect (Figure **F15**). The site is at 3544 m water depth and will penetrate 435 mbsf, including 365 m of sediment and 70 m of basement. As with the other Vavilov Basin sites, the primary objective is to recover mantle peridotites. In Hole A, we will RCB core with recovery through the sediment to the target depth in the basement (70 m subbasement), take three temperature measurements with the SET2 tool during coring, and then log the hole with the triple combo and FMS-sonic tool strings. This selected depth of basement penetration may cross the exhumation fault zone, but balances coring time with priority operations at other sites. If recovery of the sediment/basement interface was poor or recovered material was low quality, we will drill down to 315 mbsf with the APC/XCB system in Hole B, and then capture the lowermost 50 m of sediment and the sediment/basement interface via XCB coring. This second sample of the sediment/basement interface ensures adequate material for dating and for biogeochemical studies

**Site Figure** **IODP proposal P927** **Site TYR-12A**

| | |
|---|---|
| Priority: | Primary |
| Position: | 40.4159° N; 12.7076° E<br>Abyssal plan of Vavilov Basin |
| Water depth (m): | 3590 |
| Target drilling depth (mbsf): | 723 |
| Approved maximum penetration (mbsf): | Discretion of shipboard party to deepen the hole if time is available |
| Survey coverage (track map; seismic profile): | Medoc11_8250-15750.sgy (CDP 12198) |
| Objective(s): | Recovery of peridotite underneath Plio-Quaternary sediments deposits |
| Coring program: | Hole A: APC/XCB of the whole sedimentary cover plus 5 m into the basement<br>Hole B: RCB from the deepest 50 m of sediment to total depth |
| Downhole measurements program: | Hole B: Wireline log with triple combo, FMS-sonic |
| Nature of rock anticipated: | 653 m of terrigenous sand/silt/clay followed by70 m of serpentinized mantle rocks |

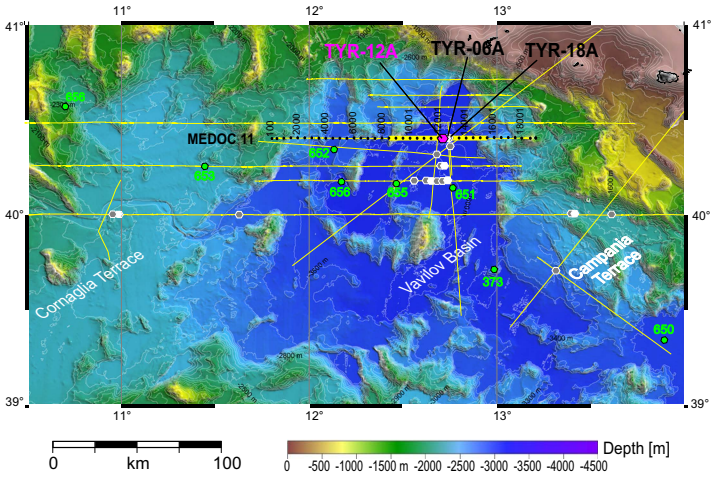


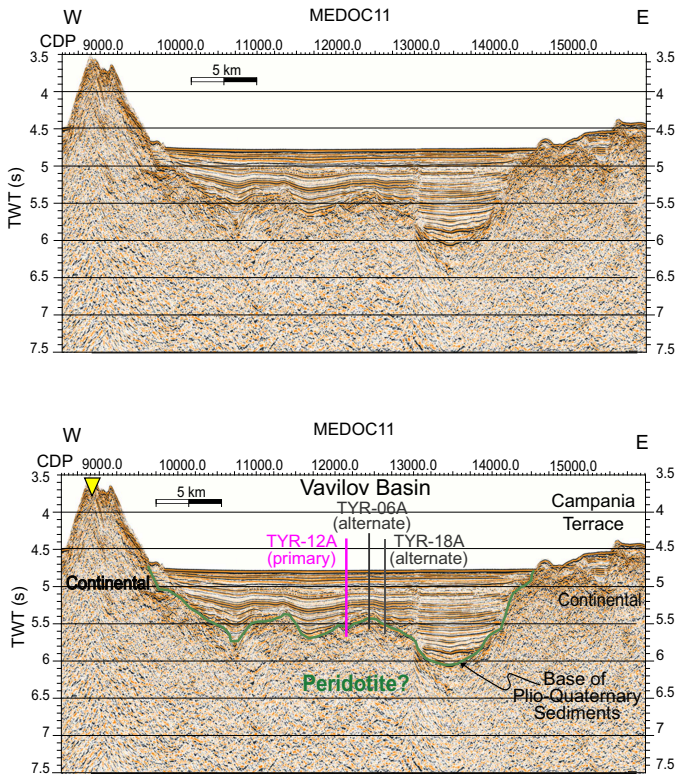


**Figure F13.** Site TYR-12A and one of its alternates, TYR-18A. Bottom right seismic line panel: interpreted sediment-basement interface, site locations, and approximate planned penetration are shown. The drilling target is the rocks located below the base of the Pliocene–Quaternary sediments (green line). CDP = common depth point, TWT = two-way traveltime.

## Site Figure IODP proposal P927 Site TYR-19A

| | |
|---|---|
| Priority: | Alternateof TYR-12A |
| Position: | 40.38562° N; 12.74428°E<br>Vavilov Basin |
| Water depth (m): | 3601 |
| Target drilling depth (mbsf): | 1133 |
| Approved maximum penetration (mbsf): | Discretion of shipboard party to deepen the hole if time is available |
| Survey coverage (track map; seismic profile): | M29B_TYR17A_CDP12361-14750.sgy (CDP 13690); ST03A_TYR19A_CDP4228-5132.sgy (CDP 4535) |
| Objective(s): | Recovery of peridotite underneath Plio-Quaternary sediments deposits |
| Coring program: | Hole A: APC/XCB of the whole sedimentary cover plus 5 m into the basement<br>Hole B: RCB from the deepest 50 m of sediment to total depth |
| Downhole measurements program: | Hole B: Wireline log with triple combo, FMS-sonic |
| Nature of rock anticipated: | 1063 m of terrigenous sand/silt/clay plus 70 m of serpentinized mantle rocks |

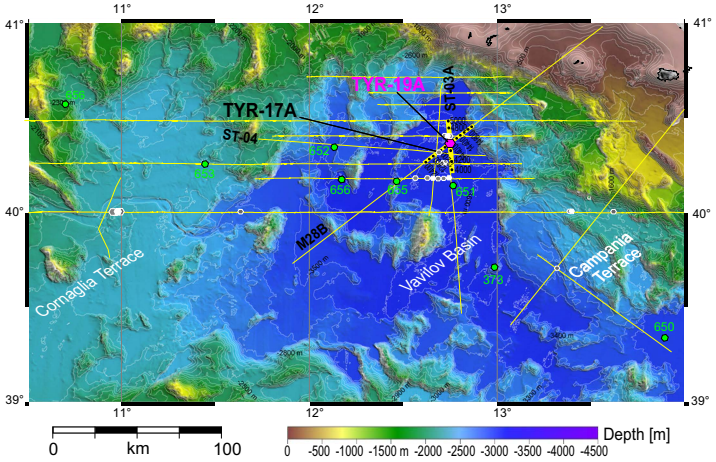


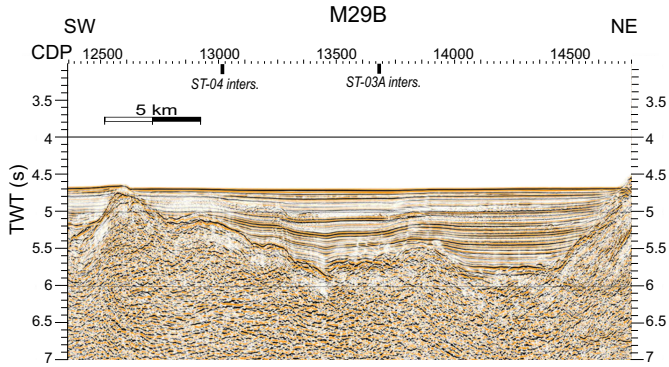


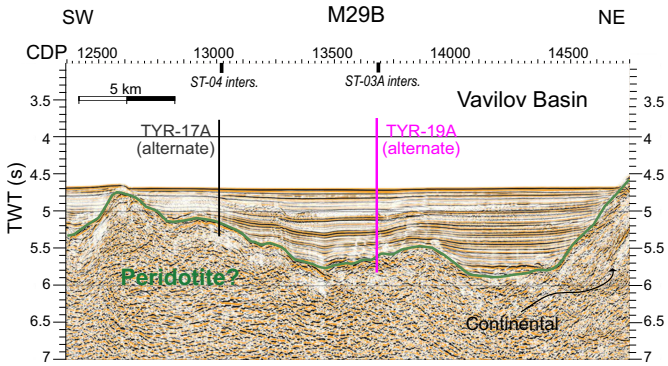


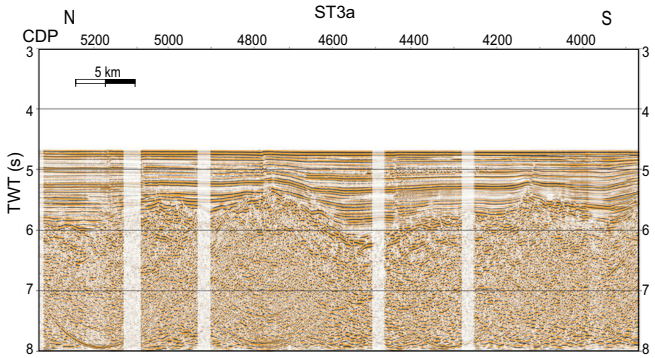


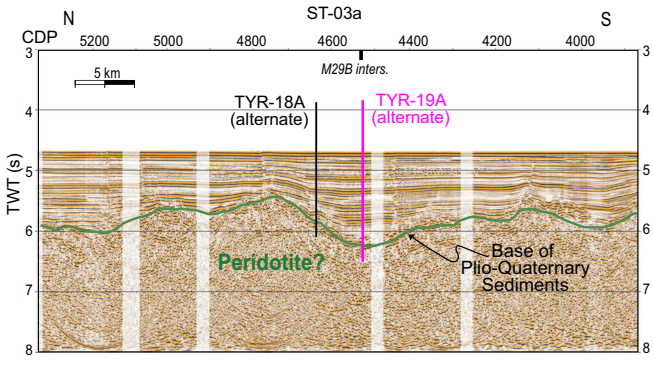


**Figure F14.** Site TYR-19A, alternate of TYR-12A. Bottom right seismic line panel: interpreted sediment-basement interface, site location, and approximate planned penetration are shown. The drilling target is the rocks located below the base of the Pliocene–Quaternary sediments (green line). CDP = common depth point, TWT = two-way traveltime.

of serpentinization reactions. Alternate Sites TYR-4A and TYR-16A lie along either side of the primary Site TYR-10A on the same seismic line (Figure **F15**). Alternate sites will be drilled with the same strategy. Site TYR-4A is located at 3546 mbsf and the plan is to RCB core to 548 mbsf (478 m sediments plus 70 m serpentinized peridotites), followed by a second APC/XCB hole to recover the 50 m sediment overlying basement and the interface as time allows. Site TYR-16 is located at 3578 mbsf and the plan is to RCB core to 341 mbsf (271 m sediments plus 70 m serpentinized peridotites), again followed by a second hole to recover the sediment/basement interface as time allows.

Site TYR-11A (alternates: Sites TYR-5A and TYR-17A) (Figures **F16**, **F17**) will be drilled last during Expedition 402, following completion of Site TYR-2A on the Campania Terrace (strategy described in the next section). The site has a water depth of 3538 m and an estimated sediment cover of 202 m. Drilling at Site TYR-11A completes the north–south transect and targets mantle peridotites. As with the other Vavilov Basin sites, the operations plan involves coring a Hole A with the RCB system through sediment to 140 m subbasement, taking three temperature measurements with the SET2 tool during coring, and then logging the hole with the triple combo and FMS-sonic tool strings. This depth of basement penetration will theoretically cross the exhumation fault zone at ~100 m or less below the top of basement (Escartín et al., 2017). Although the site is higher priority than Site TYR-2A, it will be drilled last so that any remaining expedition time can be spent deepening the hole beyond 140 m subbasement. If recovery of the sediment/basement interface in Hole A was poor, a second hole will drill down to 152 mbsf using

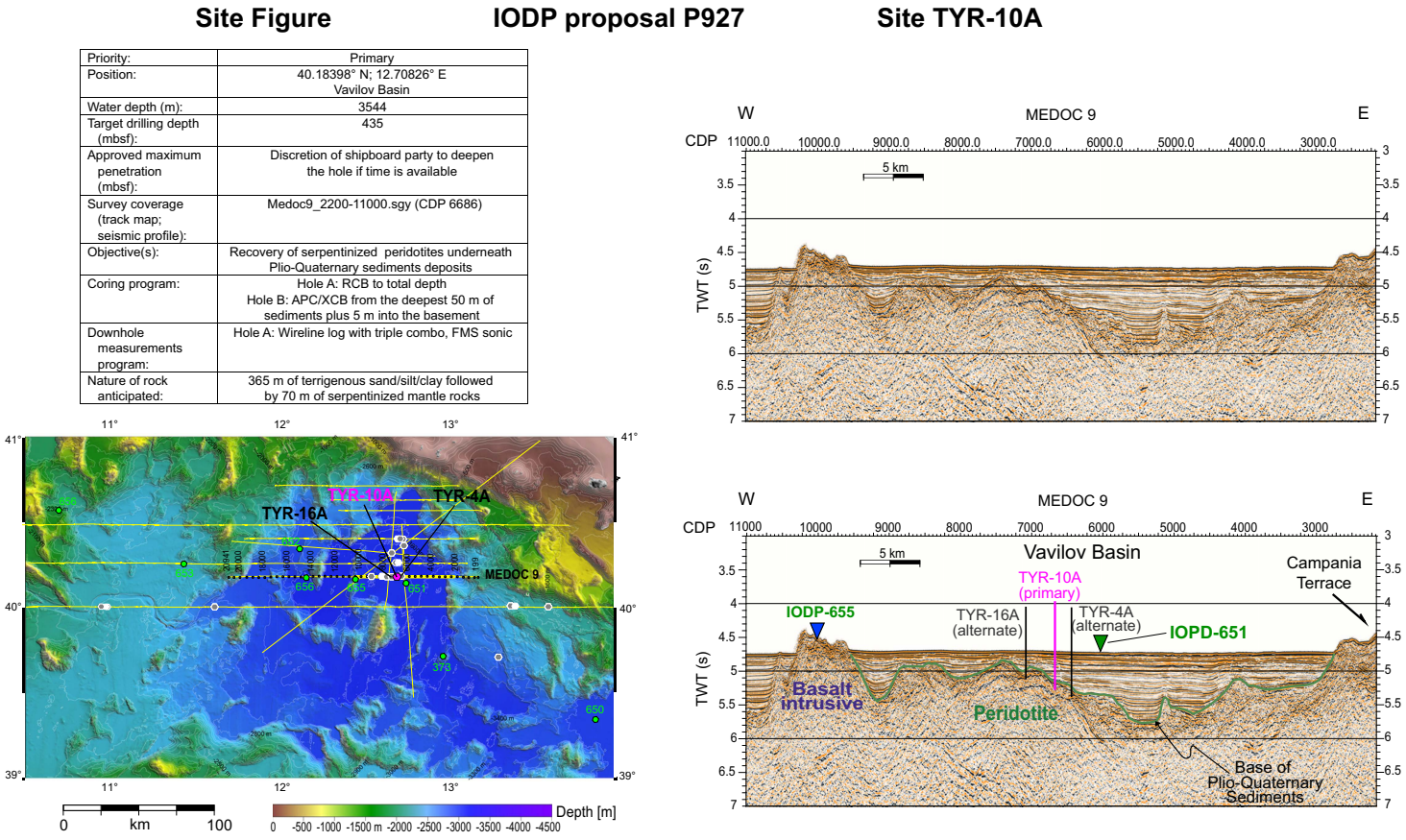


**Figure F15.** Site TYR-10A and its alternates, TYR-04A and TYR-16A. Bottom seismic line panel: interpreted sediment-basement interface, site location, and approximate planned penetration are shown. The drilling target is the rocks located below the base of the Pliocene–Quaternary sediments (green line). CDP = common depth point, TWT = two-way traveltime.

the APC/XCB coring system, followed by coring the lowermost 50 m of sediment to reach the sediment/basement interface. Alternate Site TYR-5A is adjacent to Site TYR-11A on the same seismic line and has a similar water depth but thinner sediment cover (88 m) (Figure **F16**). At Site TYR-5A, Hole A would be cored to 228 m with the RCB system and logged, followed by a second hole using the APC/XCB system to recover the sediment/basement interface as time allows. Alternate Site TYR-17A is located at the intersection of MCS Lines ST-04 and M29B (Figure **F17**). It sits in slightly deeper water (3600 m) and has a greater sediment cover. Planned operations involve coring to 602 m with the RCB system (462 m sediment plus 140 m serpentinized peridotites), logging with the triple combo and FMS-sonic tool strings, and then recovering the sediment/basement interface, including 50 m of sediment overlying basement, with the APC/XCB coring system, as time allows.

### 5.1.2. Preexhumation basalts on the Cornaglia and Campania Terraces

Sites TYR-7A and TYR-2A are at the two opposite ends of the west–east transect and target pre-exhumation basalts on the Cornaglia and Campania Terraces, respectively (Figure **F1**). At both of these sites, a single hole will be cored to 70 m subbasement using the RCB coring system. Three

**Site Figure** **IODP proposal P927** **Site TYR-11A**

| | |
|---|---|
| Priority: | Primary |
| Position: | 40.26614° N; 12.70529° E<br>Vavilov Basin |
| Water depth (m): | 3538 |
| Target drilling depth (mbsf): | 342 |
| Approved maximum penetration (mbsf): | Discretion of shipboard party to deepen the hole if time is available |
| Survey coverage (track map; seismic profile): | Medoc8_35250-43000.sgy (CDP 39749) |
| Objective(s): | Recovery of serpentinized peridotite underneath Plio-Quaternary sediments deposits |
| Coring program: | Hole A: RCB to total depth<br>Hole B: APC/XCB from the deepest 50 m of sediments plus 5 m. into the basement |
| Downhole measurements program: | Hole A: Wireline log with triple combo, FMS-sonic |
| Nature of rock anticipated: | 202 m of terrigenous sand/silt/clay followed by 140 m into the serpentinized mantle peridotite |

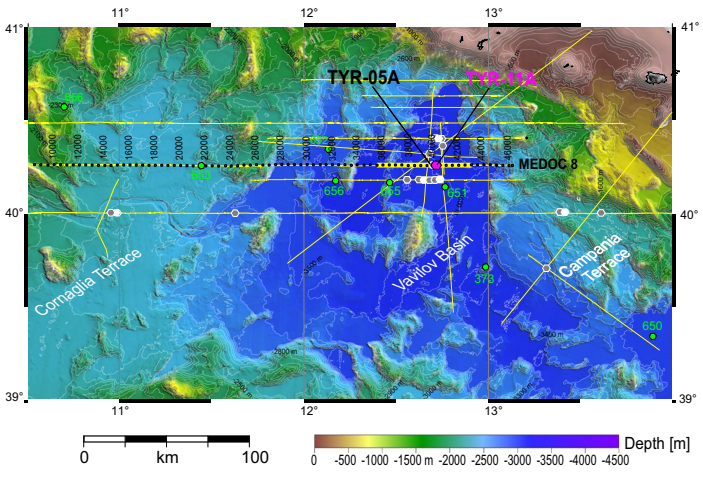


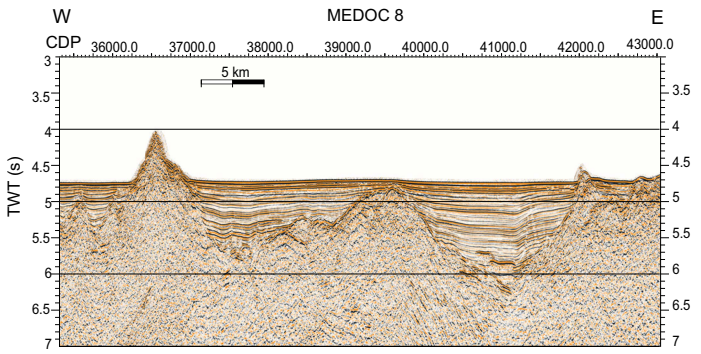


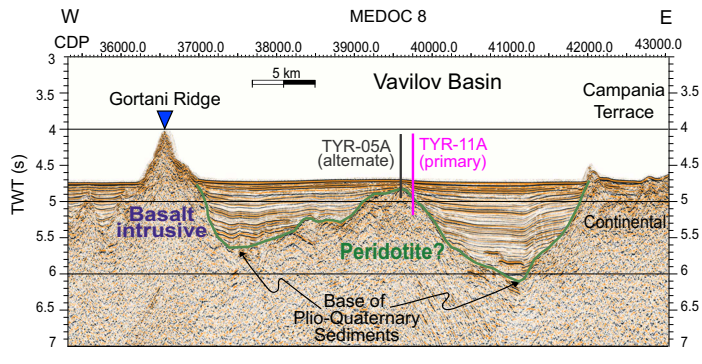


**Figure F16.** Site TYR-11A and its alternate, TYR-05A. Bottom seismic line panel: interpreted sediment-basement interface, site locations, and approximate planned penetration are shown. The drilling target is the rocks located below the base of the Pliocene–Quaternary sediments (green line). CDP = common depth point, TWT = two-way traveltime.

temperature measurements will be made with the SET2 tool during coring; the hole will then be logged with the triple combo and FMS-sonic tool strings.

Site TYR-7A on the Cornaglia Terrace has a water depth of 2700 m; RCB drilling will penetrate to 265 m total depth, including 195 m sediment and 70 m basement (Figure **F18**). Recovering the sediment/basement interface at Site TYR-7A is important as the basal sediment contains possible Messinian deposits. Three temperature measurements will be made with the SET2 tool during coring, and the hole will be logged with the triple combo and FMS-sonic tool strings after the

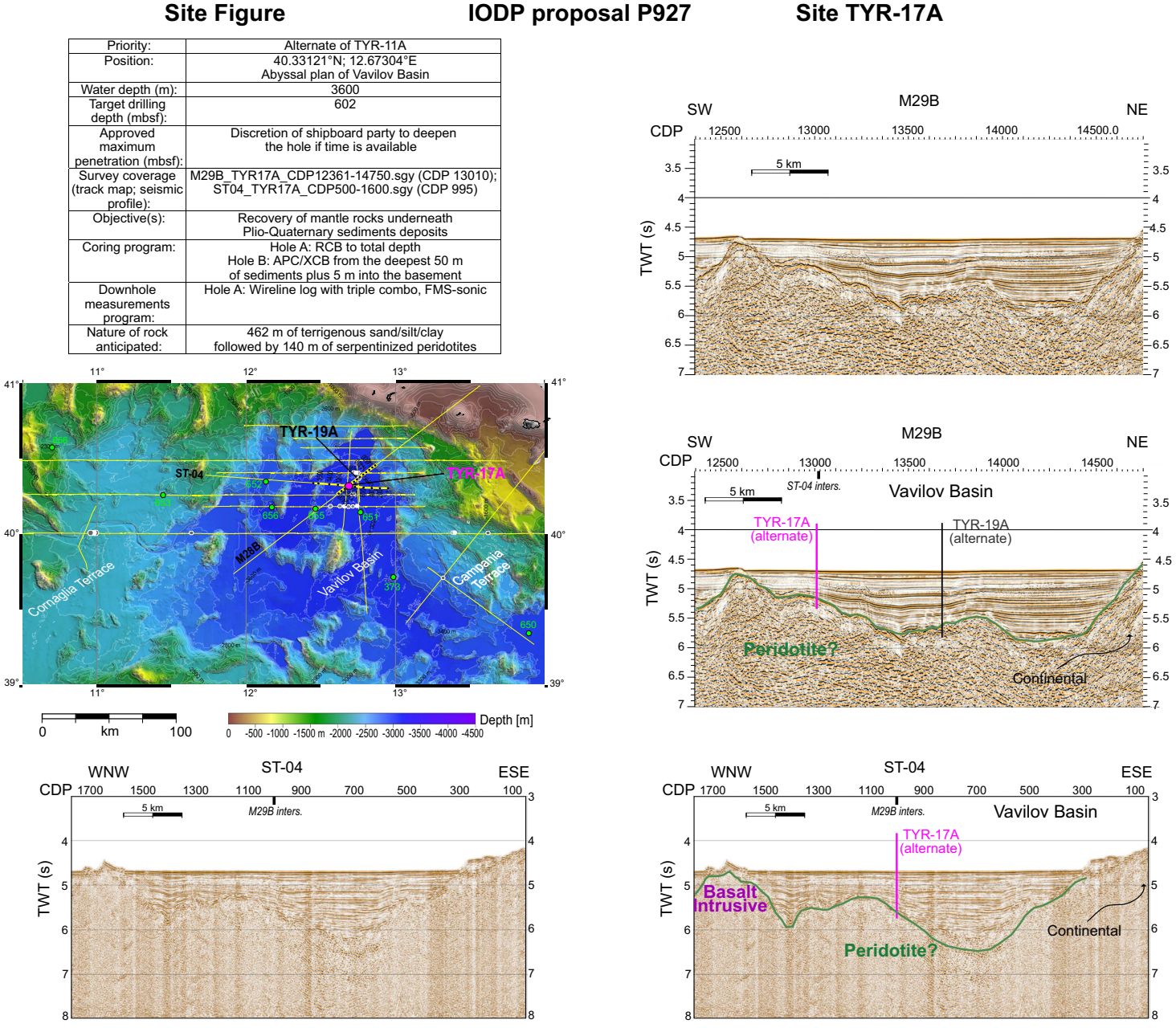


**Figure F17.** Site TYR-17A, alternate of TYR-11A. Bottom right seismic line panel: interpreted sediment-basement interface, site location, and approximate planned penetration are shown. The drilling target is the rocks located below the base of the Pliocene–Quaternary sediments (green line). CDP = common depth point, TWT = two-way traveltime.

target depth is reached. Alternate Sites TYR-1A and TYR-13B are adjacent to Site TYR-7A on the same seismic line and in similar water depths (Figure **F18**). Site TYR-1A is at 2675 m water depth, and the single planned hole will be drilled using the RCB system to a depth of 234 mbsf (164 m sediment plus 70 m basement). Site TYR-13B has a water depth of 2713 m and substantially thicker sediment cover, including 200 m of clastic sediments plus 110 m of Messinian deposits. The single RCB hole will penetrate to 380 mbsf in total, recovering the 310 m of sediment and 70 m of basement prior to logging.

Site TYR-2A on the Campania Terrace has a water depth of 2813 m; drilling in the single planned RCB hole will penetrate to 530 m total depth, including 460 m sediment and 70 m basement (Figure **F19**). Recovering the sediment/basement interface at Site TYR-2A is important as the basal sediment contains possible Messinian deposits. Three temperature measurements will be made with the SET2 tool during coring, and the hole will be logged with the triple combo and FMS-

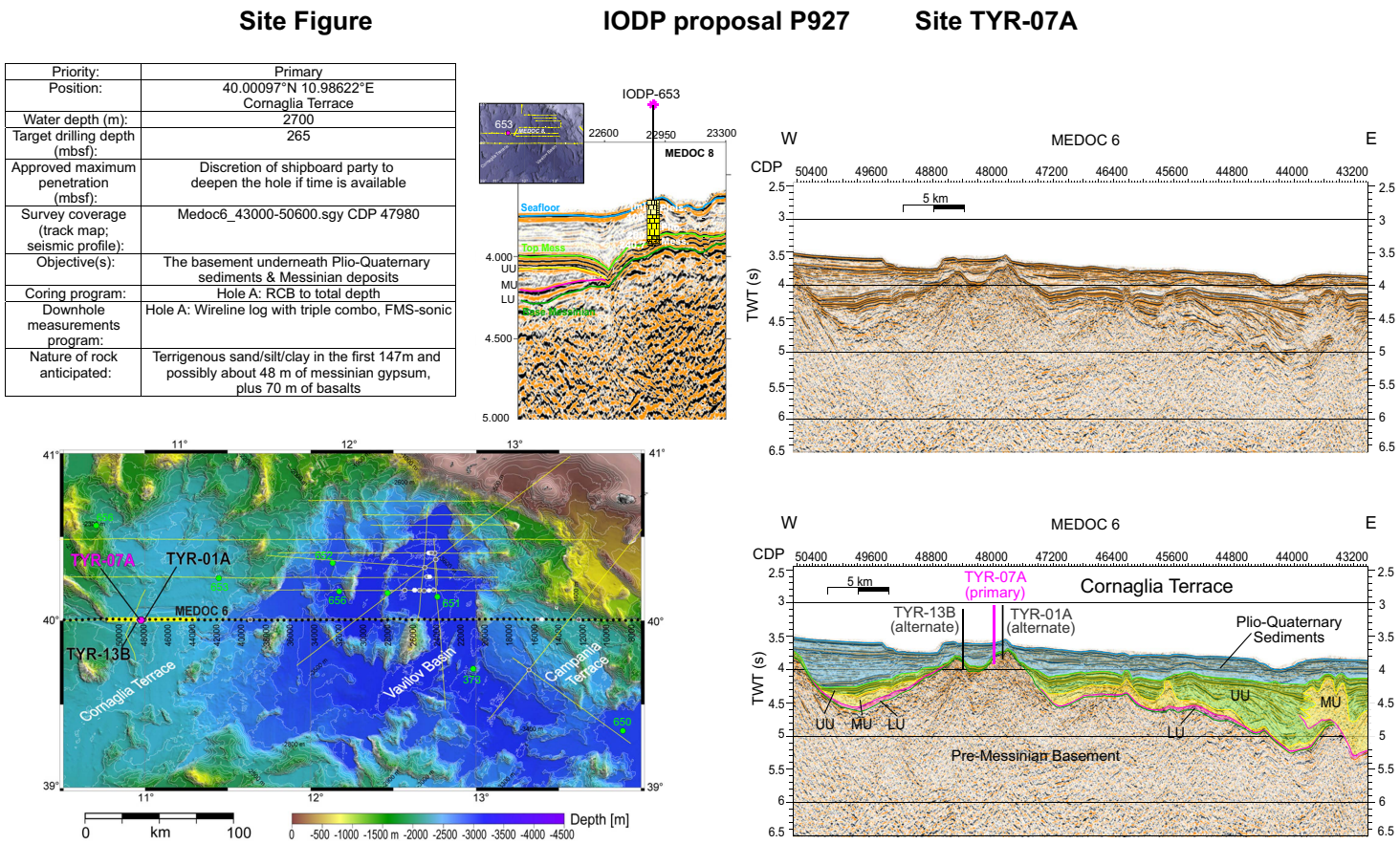


**Figure F18.** Site TYR-07A and its alternates, TYR-01A and TYR-13B. Bottom seismic line panel: interpreted sediment-basement interface, site locations, and approximate planned penetration are shown. The drilling target are the basaltic rocks located below the base of the Messinian sediments (purple line). Upper center: interpreted seismic data and sediment lithostratigraphy of the Pliocene–Quaternary and Messinian deposits at Site 653. CDP = common depth point, TWT = two-way traveltime, UU = upper unit, MU = mobile unit, LU = lower unit.

sonic tool strings after the target depth is reached. Alternate Sites TYR-8A and TYR-20A are adjacent to Site TYR-2A on the same seismic line and in similar water depths (Figure **F19**). Site TYR-8A is nearly identical to TYR-2A, with planned penetration of 524 m, including 454 m of sediment and 70 m basement. Site TYR-20A has a water depth of 2698 m and a slightly thinner sediment cover; drilling with the RCB system at that alternate site will penetrate 400 m sediment and 70 m basement prior to logging. Alternate Site TYR-14A is slightly downslope of the terrace at a water depth of 3381 m, but should still capture the basalts targeted at this site. The site is located at the intersection of Seismic Lines CROP_M30 and M2A-4 (Figure **F20**). If drilled, planned operations involve a single hole with the RCB system cored to 566 mbsf, including 496 m of sediment and 70 m of basalt. Three temperature measurements will be taken with the SET2 tool during coring and, at all alternate sites, the hole will be logged with the triple combo and FMS-sonic tool strings after the target depth is reached.

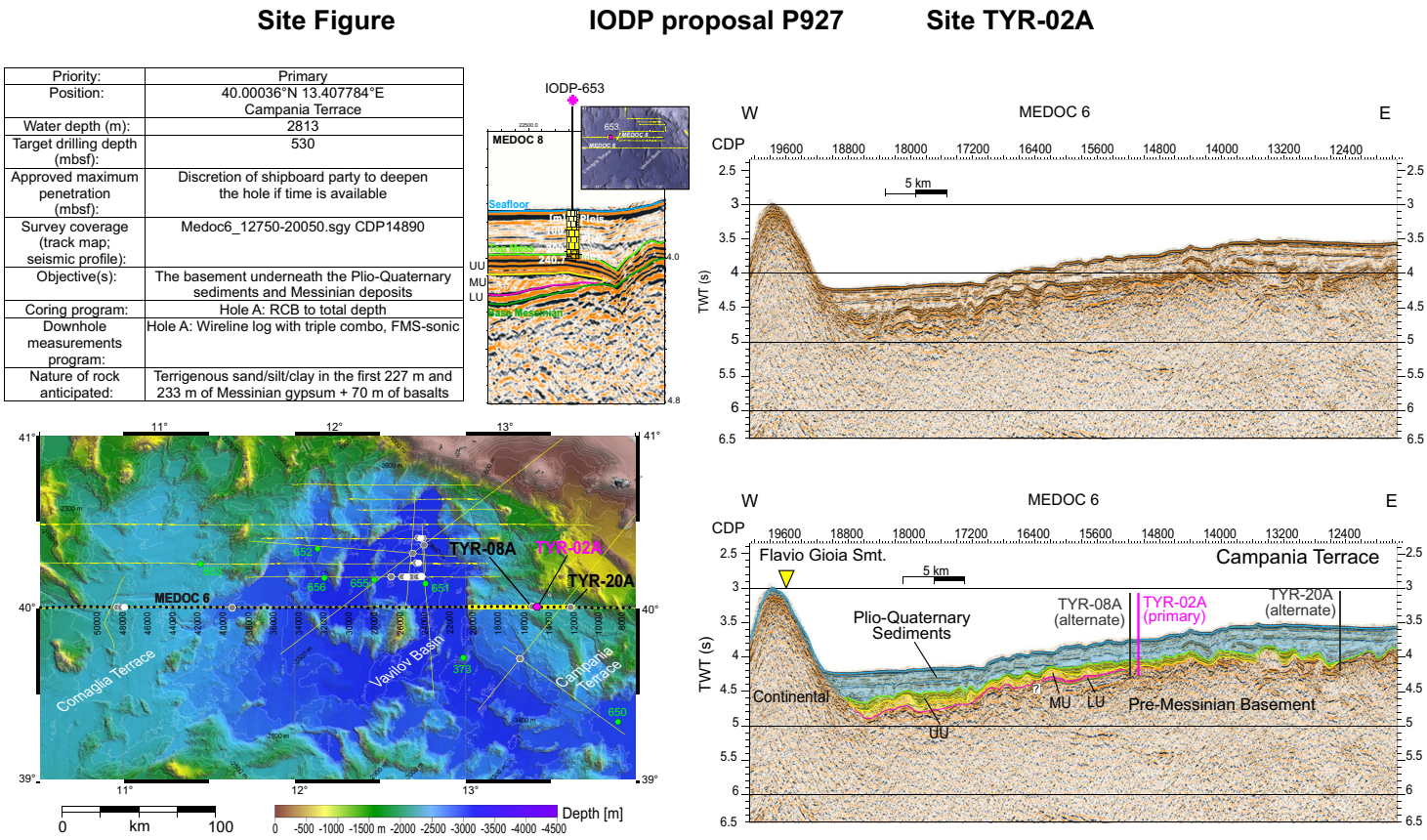


**Figure F19.** Site TYR-02A and its alternates, TYR-08A and TYR-20A. Bottom seismic line panel: interpreted sediment-basement interface, site locations, and approximate planned penetration are shown. The drilling targets are the basaltic rocks located below the base of the Messinian sediments (purple line). Upper center: interpreted seismic data and sediment lithostratigraphy of the Pliocene–Quaternary and Messinian deposits at Site 653. CDP = common depth point, TWT = two-way traveltime, UU = upper unit, MU = mobile unit, LU = lower unit.

**Site Figure** **IODP proposal P927** **Site TYR-14A**

| | |
|---|---|
| Priority: | Alternate of TYR-02A |
| Position: | 39.71273°N; 13.31500°E<br>Campania Terrace |
| Water depth (m): | 3381 |
| Target drilling depth (mbsf): | 566 |
| Approved maximum penetration (mbsf): | Discretion of shipboard party to deepen the hole if time is available |
| Survey coverage (track map; seismic profile): | M2A4_TYR-14A_CDP500-2100.sgy (CDP 5963); M30_TYR14A_CDP10750-12700.sgy (CDP 11626) |
| Objective(s): | Recovery of basalts underneath Plio-Quaternary sediments deposits |
| Coring program: | Hole A: RCB to total depth |
| Downhole measurements program: | Hole A: Wireline log with triple combo, FMS-sonic |
| Nature of rock anticipated: | 496 m of terrigenous sand/silt/clay followed by 70 m of basalts |

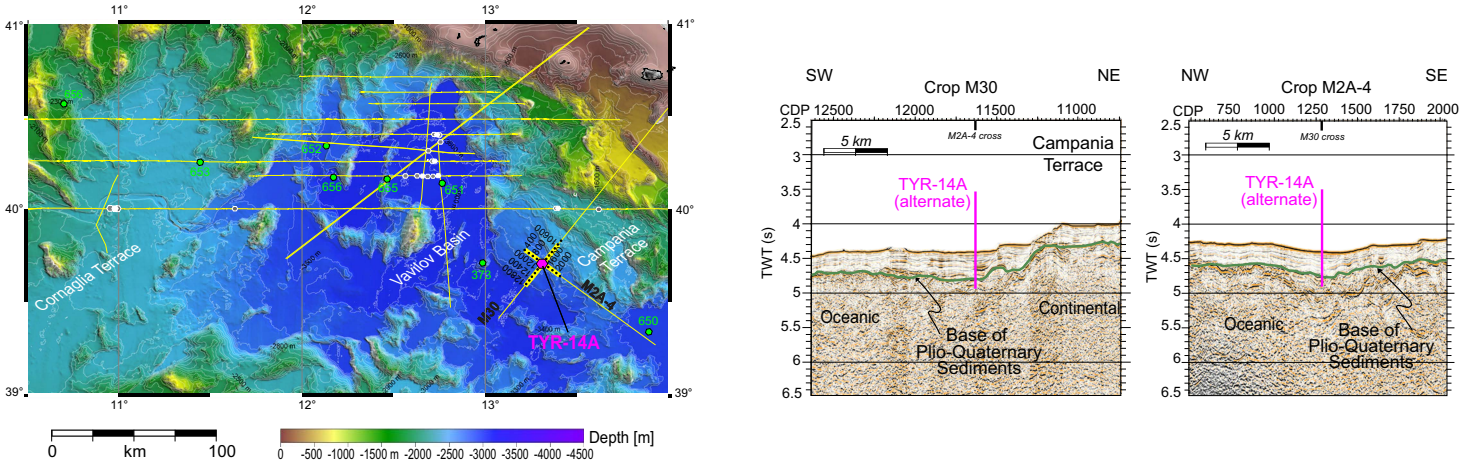


**Figure F20.** Site TYR-14A, alternate of TYR-02A. Bottom seismic line panels: interpreted sediment-basement interface, site locations, and approximate planned penetration are shown. The drilling targets are the basaltic rocks located below the base of the Pliocene–Quaternary sediments (green line). CDP = common depth point, TWT = two-way traveltime.

# 6. Wireline logging and downhole measurements strategy

Wireline logging will be important to address the scientific objectives of Expedition 402, in particular to complement core recovery in the basement rocks. Downhole logs will be acquired at all sites, typically in the hole cored with the RCB system. Two logging tool strings will be deployed:

1. A triple combo string with tools for spectral natural gamma, litho-density, and electrical resistivity measurements. Resistivity should be measured with a High-Resolution Laterolog Array (HRLA), which is expected to give the best results in high-resistivity basement rocks.
2. A FMS-sonic string with tools for spectral natural gamma, $V_P$ and $S$-wave velocities (Dipole Sonic Imager [DSI]), and electrical resistivity imaging (FMS). The natural gamma measurements will help to characterize the lithology and will allow for a precise correlation with the logging data acquired by the triple combo tool string. The in situ $V_P$ measurements will be used to tie depth in the borehole with seismic travel time. $V_P$ combined with the bulk densities measured with the triple combo tool string can be used to compute a synthetic seismogram for detailed correlation between the borehole and seismic reflection traces. The FMS resistivity images will help in the interpretation of structures such as fractures and veins in basement rocks where recovery will likely be incomplete. As a possible alternative to the FMS, we plan to run at the base of this tool string a UBI, whose rotating transducer measures a full-coverage

image of the borehole radius and borehole wall acoustic reflectivity (see Malinverno et al., 2016, for an example of UBI images obtained during IODP Expedition 344).

In addition to wireline logging, we plan to obtain in situ downhole temperature measurements at 3–4 depths spanning approximately the top 100 m of the sediment column, to determine the local geothermal gradient and heat flow and to detect potential fluid flow or active (exothermic) serpentinization processes. Temperature measurements will predominantly be taken with the SET2 tool during RCB coring, although the advanced piston corer temperature (APCT-3) tool may be used during APC coring at Site TYR-12A (Figure **F10**; Table **T1**). Technical details on the wireline logging and temperature tools used aboard *JOIDES Resolution* are at **https://iodp.tamu.edu/tools** and **https://iodp.tamu.edu/tools/logging**.

# 7. Risks and contingency

We identified the following potential risks associated with Expedition 402 that have been mitigated to the extent possible:

- Weather and sea state: storm conditions or heave that prohibits drilling will result in lost operational time. The statistics for wave height and period for a whole year in the Tyrrhenian Sea (loaded in the SSDB) give 1% probability for waves higher than 5 m. As such, we have not factored in contingency time for waiting on weather.
- Manmade hazards/risks: numerous underwater communication cables exist in the region, which require interacting with cable companies to verify approved operating distances. No companies have yet responded with concerns about the locations of proposed sites.
- Shipping lanes: the drilling sites are not located along main commercial ship routes, nevertheless *JOIDES Resolution* operations should be communicated in advance to the competent institution that broadcasts Notices to Mariners.
- Natural hazards: the seismic lines do not show evidence of free gas or fluid flow affecting the sedimentary sequence at the proposed sites; thus, we consider shallow drilling hazards to be minimal. At all proposed sites, we have received approval from the Environmental Protection and Safety Panel (EPSP) to deepen holes beyond the target depth as time is available.
- Recovery: approximately 2.3 km of core is expected to be recovered during Expedition 402. Transit times between sites are very short, leaving minimal time for maintenance, catch-up, or downtime.
- Clearance: the drilling sites are in Italy's Exclusive Economic Zone, and obtaining clearance to drill will be necessary.

None of these factors pose major risks to the operations plan outlined in Table **T1**; as such, we do not include contingency time. The plan has flexibility in that the sites will be drilled in priority order, with the exception of scheduling Site TYR-11A last. That site will be drilled last such that any remaining operations time can be applied to deepening the hole. However, if the expedition is behind schedule, operations at other sites may be curtailed to allow enough time to complete basic operations at Site TYR-11A. Time can also be saved by not drilling a Hole B with the APC/XCB system to recover a second sample of the sediment/basement interface at all sites except TYR-12A (Figure **F10**; Table **T1**; see **Operations plan and coring strategy**).

# 8. Sampling and data sharing strategy

Shipboard and shore-based researchers should refer to the IODP Sample, Data, and Obligations Policy and Implementation Guidelines posted on the Web at **https://www.iodp.org/top-resources/program-documents/policies-and-guidelines**. This document outlines the policy for distributing IODP samples and data to research scientists, curators, and educators. The document also defines the obligations that sample and data recipients incur. The Sample Allocation Committee (SAC; composed of the Co-Chief Scientists, Staff Scientist, and IODP Curator on shore and curatorial representative on board the ship) will work with the entire scientific party to formulate a formal expedition-specific sampling plan for shipboard and any postcruise sampling. Every

member of the science party is obligated to carry out scientific research for the expedition and publish the results.

Shipboard scientists are expected to submit sample requests (at **https://iodp.tamu.edu/curation/samples.html**) ~6 months before the beginning of the expedition. Based on sample requests (shore-based and shipboard) submitted by this deadline, the SAC will prepare a tentative sampling plan, which will be revised on the ship as dictated by core recovery and cruise objectives. The sampling plan will be subject to modification depending upon the actual material recovered and collaborations that may evolve between scientists during the expedition. Modification of the strategy during the expedition must be approved by the Co-Chief Scientists, Staff Scientist, and curatorial representative on board the ship. All sample frequencies and sizes must be justified on a scientific basis and will depend on core recovery, the full spectrum of other requests, and the cruise objectives. Some redundancy of measurement is unavoidable, but minimizing the duplication of measurements among the shipboard party and identified shore-based collaborators will be a factor in evaluating sample requests.

If any critical intervals are recovered, there may be considerable demand for samples from a limited amount of cored material. These intervals may require special handling, a higher sampling density, reduced sample size, or continuous core sampling by a single investigator. A sampling plan coordinated by the SAC may be required before critical intervals are sampled. The minimum permanent archive will be the standard archive half of each core.

Shipboard sampling will include samples taken for shipboard analyses as well as samples requested for personal postexpedition research. No shore-based sample party is currently planned for Expedition 402. We expect a large number of shipboard and personal whole-round samples will be collected for geochemical, petrophysical, and possibly microbiological measurements.

The cores from Expedition 402 will be delivered to the Bremen Core Repository (BCR) for permanent storage. Archive halves may first travel to the Gulf Coast Repository (GCR) in College Station (USA) or the Center for Marine Environmental Sciences (MARUM) at the University of Bremen (Germany) for postcruise programmatic X-ray fluorescence (XRF) core scanning.

All collected cores, data, and samples will be protected by a 1 y moratorium period that will start at the end of the expedition. During this moratorium, only expedition shipboard scientists and approved shore-based participants will be allowed to access expedition data and samples.

# 9. Expedition scientists and scientific participants

The current list of participants for Expedition 402 can be found at **https://iodp.tamu.edu/scienceops/expeditions/tyrrhenian_continent_ocean_transition.html**.

# References

AGIP and SGN (Servizio Geologico Nazionale), 1994. Carta Aeromagnetica d'Italia, Scala 1:1000000 Italy: Istituto Poligrafico Zecca dello Stato.

Andreani, M., and Ménez, B., 2019. New perspectives on abiotic organic synthesis and processing during hydrothermal alteration of the oceanic lithosphere. In Orcutt, B.N., Daniel, I., and Dasgupta, R. (Eds.), Deep Carbon: Past to Present. Cambridge (Cambridge University Press), 447–479. **https://doi.org/10.1017/9781108677950**

Andreani, M., Mével, C., Boullier, A.M., and Escartín, J., 2007. Dynamic control on serpentine crystallization in veins; constraints on hydration processes in oceanic peridotites. Geochemistry, Geophysics, Geosystems, 8(2):Q02012. **https://doi.org/10.1029/2006GC001373**

Andreani, M., Muñoz, M., Marcaillou, C., and Delacour, A., 2013. μXANES study of iron redox state in serpentine during oceanic serpentinization. Lithos, 178:70–83. **https://doi.org/10.1016/j.lithos.2013.04.008**

Andrés-Martínez, M., Pérez-Gussinyé, M., Armitage, J., and Morgan, J.P., 2019. Thermomechanical Implications of Sediment Transport for the Architecture and Evolution of Continental Rifts and Margins. Tectonics, 38(2):641–665. **https://doi.org/10.1029/2018TC005346**

Argnani, A., and Savelli, C., 1999. Cenozoic volcanism and tectonics in the southern Tyrrhenian sea: space-time distribution and geodynamic significance. Journal of Geodynamics, 27(4):409–432. **https://doi.org/10.1016/S0264-3707(98)00025-8**

Bach, W., Garrido, C.J., Paulick, H., Harvey, J., and Rosner, M., 2004. Seawater-peridotite interactions: first insights from ODP Leg 209, MAR 15°N. Geochemistry, Geophysics, Geosystems, 5(9):Q09F26. **https://doi.org/10.1029/2004GC000744**

Beccaluva, L., Bonatti, E., Dupuy, C., Ferrara, G., Innocenti, F., Lucchini, F., Macera, P., Petrini, R., Rossi, P.L., Serri, G., Seyler, M., and Siena, F., 1990. Geochemistry and mineralogy of volcanic rocks from ODP Sites 650, 651, 655, and 654 in the Tyrrhenian Sea. In Kastens, K.A., Mascle, J., et al., Proceedings of the Ocean Drilling Program, Scientific Results. 107: College Station, TX (Ocean Drilling Program), 49–47. **https://doi.org/10.2973/odp.proc.sr.107.140.1990**

Bertrand, H., Boivin, P., and Robin, C., 1990. Petrology and geochemistry of basalts from the Vavilov Basin (Tyrrhenian Sea), Ocean Drilling Program Leg 107, Holes 651A and 655B. In Kastens, K.A., Mascle, J., et al., Proceedings of the Ocean Drilling Program, Scientific Results. 107: College Station, TX (Ocean Drilling Program), 75–92. **https://doi.org/10.2973/odp.proc.sr.107.142.1990**

Beslier, M.O., Girardeau, J., and Boillot, G., 1990. Kinematics of peridotite emplacement during North Atlantic continental rifting, Galicia, northwestern Spain. Tectonophysics, 184(3):321–343. **https://doi.org/10.1016/0040-1951(90)90446-F**

Bodinier, J.L., and Godard, M., 2007. 2.04 - Orogenic, Ophiolitic, and Abyssal Peridotites. In Holland, H.D. and Turekian, K.K., Treatise on Geochemistry. Oxford (Pergamon), 1–73. **https://doi.org/10.1016/B0-08-043751-6/02004-1**

Boillot, G., and Winterer, E.L., 1988. Drilling on the Galicia margin: retrospect and prospect. In Boillot, G., Winterer, E. L., et al., Proceedings of the Ocean Drilling Program, Scientific Results. 103: College Station, TX (Ocean Drilling Program), 809–828. **https://doi.org/10.2973/odp.proc.sr.103.180.1988**

Bonatti, E., Seyler, M., Channell, J.E.T., Giraudeau, J., and Mascle, G., 1990. Peridotites drilled from the Tyrrhenian Sea, ODP Leg 107. In Kastens, K.A., Mascle, J., et al., Proceedings of the Ocean Drilling Program, Scientific Results. 107: College Station, TX (Ocean Drilling Program), 37–47. **https://doi.org/10.2973/odp.proc.sr.107.141.1990**

Bonnemains, D., Carlut, J., Escartín, J., Mével, C., Andreani, M., and Debret, B., 2016. Magnetic signatures of serpentinization at ophiolite complexes. Geochemistry, Geophysics, Geosystems, 17(8):2969–2986. **https://doi.org/10.1002/2016GC006321**

Brunelli, D., Seyler, M., Cipriani, A., Ottolini, L., and Bonatti, E., 2006. Discontinuous Melt Extraction and Weak Refertilization of Mantle Peridotites at the Vema Lithospheric Section (Mid-Atlantic Ridge). Journal of Petrology, 47(4):745–771. **https://doi.org/10.1093/petrology/egi092**

Cameselle, A.L., Ranero, C.R., Franke, D., and Barckhausen, U., 2017. The continent-ocean transition on the northwestern South China Sea. Basin Research, 29(S1):73–95. **https://doi.org/10.1111/bre.12137**

Cannat, M., Sauter, D., Bezos, A., Meyzen, C., Humler, E., and Le Rigoleur, M., 2008. Spreading rate, spreading obliquity, and melt supply at the ultraslow spreading Southwest Indian Ridge. Geochemistry, Geophysics, Geosystems, 9(4). **https://doi.org/10.1029/2007GC001676**

Caratori Tontini, F., Stefanelli, P., Giori, I., Faggioni, O., Carmisciano, C., 2004. The revised aeromagnetic anomaly map of Italy. Annals of Geophysics, 47(5). **https://doi.org/10.4401/ag-3358**

Cipriani, A., Bonatti, E., Seyler, M., Brueckner, H.K., Brunelli, D., Dallai, L., Hemming, S.R., Ligi, M., Ottolini, L., and Turrin, B.D., 2009. A 19 to 17 Ma amagmatic extension event at the Mid-Atlantic Ridge: Ultramafic mylonites from the Vema Lithospheric Section. Geochemistry, Geophysics, Geosystems, 10(10). **https://doi.org/10.1029/2009GC002534**

Davis, J.K., and Lavier, L.L., 2017. Influences on the development of volcanic and magma-poor morphologies during passive continental rifting. Geosphere, 13(5):1524–1540. **https://doi.org/10.1130/GES01538.1**

Davy, R.G., Minshull, T.A., Bayrakci, G., Bull, J.M., Klaeschen, D., Papenberg, C., Reston, T.J., Sawyer, D.S., and Zelt, C.A., 2016. Continental hyperextension, mantle exhumation, and thin oceanic crust at the continent-ocean transition, West Iberia: New insights from wide-angle seismic. Journal of Geophysical Research: Solid Earth, 121(5):3177–3199. **https://doi.org/10.1002/2016JB012825**

Debret, B., Albers, E., Walter, B., Price, R., Barnes, J.D., Beunon, H., Facq, S., Gillikin, D.P., Mattielli, N., and Williams, H., 2019. Shallow forearc mantle dynamics and geochemistry; new insights from IODP Expedition 366. Lithos, 326–327:230–245. **https://doi.org/10.1016/j.lithos.2018.10.038**

Debret, B., Andreani, M., Delacour, A., Rouméjon, S., Trcera, N., and Williams, H., 2017. Assessing sulfur redox state and distribution in abyssal serpentinites using XANES spectroscopy. Earth and Planetary Science Letters, 466:1–11. **https://doi.org/10.1016/j.epsl.2017.02.029**

Debret, B., Andreani, M., Godard, M., Nicollet, C., Schwartz, S., and Lafay, R., 2013. Trace element behavior during serpentinization/de-serpentinization of an eclogitized oceanic lithosphere: A LA-ICPMS study of the Lanzo ultramafic massif (Western Alps). Chemical Geology, 357:117–133. **https://doi.org/10.1016/j.chemgeo.2013.08.025**

Debret, B., Koga, K.T., Nicollet, C., Andreani, M., and Schwartz, S., 2014. F, Cl and S input via serpentinite in subduction zones: implications for the nature of the fluid released at depth. Terra Nova, 26(2):96–101. **https://doi.org/10.1111/ter.12074**

Della Vedova, B., Bellani, S., Pellis, G., and Squarci, P., 2001. Deep temperatures and surface heat flow distribution. In Vai, G.B. and Martini, I.P., Anatomy of an Orogen: the Apennines and Adjacent Mediterranean Basins. (Springer), 65–76. **https://doi.org/10.1007/978-94-015-9829-3_7**

Deschamps, F., Godard, M., Guillot, S., and Hattori, K., 2013. Geochemistry of subduction zone serpentinites: A review. Lithos, 178:96–127. **https://doi.org/10.1016/j.lithos.2013.05.019**

Deschamps, F., Guillot, S., Godard, M., Andreani, M., and Hattori, K., 2011. Serpentinites act as sponges for fluid-mobile elements in abyssal and subduction zone environments. Terra Nova, 23(3):171–178. **https://doi.org/10.1111/j.1365-3121.2011.00995.x**

Dietrich, V., Emmermann, R., Keller, J., and Puchelt, H., 1977. Tholeiitic basalts from the Tyrrhenian Sea floor. Earth and Planetary Science Letters, 36(2):285–296. **https://doi.org/10.1016/0012-821X(77)90211-4**

Duschenes, J., Sinha, M.C., and Louden, K.E., 1986. A seismic refraction experiment in the Tyrrhenian Sea. Geophysical Journal International, 85(1):139–160. **https://doi.org/10.1111/j.1365-246X.1986.tb05175.x**

EMODnet Bathymetry Consortium, 2018. EMODnet Digital Bathymetry (DTM 2018). EMODnet Bathymetry Consortium. **http://doi.org/10.12770/18ff0d48-b203-4a65-94a9-5fd8b0ec35f6**

Escartín, J., Mével, C., MacLeod, C.J., and McCaig, A.M., 2003. Constraints on deformation conditions and the origin of oceanic detachments: the Mid-Atlantic Ridge core complex at 15°45′N. Geochemistry, Geophysics, Geosystems, 4(8):1067. **https://doi.org/10.1029/2002GC000472**

Escartín, J., Mével, C., Petersen, S., Bonnemains, D., Cannat, M., Andreani, M., Augustin, N., Bezos, A., Chavagnac, V., Choi, Y., Godard, M., Haaga, K., Hamelin, C., Ildefonse, B., Jamieson, J., John, B., Leleu, T., MacLeod, C.J., Massot-Campos, M., Nomikou, P., Olive, J.A., Paquet, M., Rommevaux, C., Rothenbeck, M., Steinfuhrer, A., Tominaga, M., Triebe, L., Campos, R., Gracias, N., and Garcia, R., 2017. Tectonic structure, evolution, and the nature of oceanic core complexes and their detachment fault zones (13°20′N and 13°30′N, Mid Atlantic Ridge). Geochemistry, Geophysics, Geosystems, 18(4):1451–1482. **https://doi.org/10.1002/2016GC006775**

Escartín, J., Smith, D.K., Cann, J., Schouten, H., Langmuir, C.H., and Escrig, S., 2008. Central role of detachment faults in accretion of slow-spreading oceanic lithosphere. Nature, 455(7214):790–794. **https://doi.org/10.1038/nature07333**

Faccenna, C., Becker, T.W., Lucente, F.P., Jolivet, L., and Rossetti, F., 2001. History of subduction and back arc extension in the Central Mediterranean. Geophysical Journal International, 145(3):809–820. **https://doi.org/10.1046/j.0956-540x.2001.01435.x**

Gillard, M., Sauter, D., Tugend, J., Tomasi, S., Epin, M.-E., and Manatschal, G., 2017. Birth of an oceanic spreading center at a magma-poor rift system. Scientific Reports, 7(1):15072. **https://doi.org/10.1038/s41598-017-15522-2**

González-Jiménez, J.M., Villaseca, C., Griffin, W.L., Belousova, E., Konc, Z., Ancochea, E., O'Reilly, S.Y., Pearson, N.J., Garrido, C.J., and Gervilla, F., 2013. The architecture of the European-Mediterranean lithosphere: A synthesis of the Re-Os evidence. Geology, 41(5):547–550. **https://doi.org/10.1130/G34003.1**

Goodliffe, A.M., and Taylor, B., 2007. The boundary between continental rifting and sea-floor spreading in the Woodlark Basin, Papua New Guinea. In Karner, G.D., Manatschal, G. and Pinheiro, L.M., Imaging, Mapping and Modelling Continental Lithosphere Extension and Breakup. 282: (Geological Society of London). **https://doi.org/10.1144/SP282.11**

Harvey, J., Gannoun, A., Burton, K.W., Rogers, N.W., Alard, O., and Parkinson, I.J., 2006. Ancient melt extraction from the oceanic upper mantle revealed by Re–Os isotopes in abyssal peridotites from the Mid-Atlantic ridge. Earth and Planetary Science Letters, 244(3):606–621. **https://doi.org/10.1016/j.epsl.2006.02.031**

Herzberg, C., 2004. Geodynamic Information in Peridotite Petrology. Journal of Petrology, 45(12):2507–2530. **https://doi.org/10.1093/petrology/egh039**

Hopper, J.R., Funck, T., Tucholke, B.E., Larsen, H.C., Holbrook, W.S., Louden, K.E., Shillington, D., and Lau, H., 2004. Continental breakup and the onset of ultraslow seafloor spreading off Flemish Cap on the Newfoundland rifted margin. Geology, 32(1):93–96. **https://doi.org/10.1130/G19694.1**

Jaroslow, G.E., Hirth, G., and Dick, H.J.B., 1996. Abyssal peridotite mylonites: implications for grain-size sensitive flow and strain localization in the oceanic lithosphere. Tectonophysics, 256(1):17–37. **https://doi.org/10.1016/0040-1951(95)00163-8**

Kastens, K.A., and Mascle, J., 1990. The geological evolution of the Tyrrhenian Sea; an introduction to the scientific results of ODP Leg 107. In Kastens, K.A., Mascle, J., et al., Proceedings of the Ocean Drilling Program, Scientific Results. 107: College Station, TX (Ocean Drilling Program), 3–26. **https://doi.org/10.2973/odp.proc.sr.107.187.1990**

Klein, F., Bach, W., Humphris, S.E., Kahl, W.-A., Jöns, N., Moskowitz, B., and Berquó, T.S., 2014. Magnetite in seafloor serpentinite—Some like it hot. Geology, 42(2):135–138. **https://doi.org/10.1130/G35068.1**

Larsen, H.C., Mohn, G., Nirrengarten, M., Sun, Z., Stock, J., Jian, Z., Klaus, A., Alvarez-Zarikian, C.A., Boaga, J., Bowden, S.A., Briais, A., Chen, Y., Cukur, D., Dadd, K., Ding, W., Dorais, M., Ferré, E.C., Ferreira, F., Furusawa, A., Gewecke, A., Hinojosa, J., Höfig, T.W., Hsiung, K.H., Huang, B., Huang, E., Huang, X.L., Jiang, S., Jin, H., Johnson, B.G., Kurzawski, R.M., Lei, C., Li, B., Li, L., Li, Y., Lin, J., Liu, C., Liu, C., Liu, Z., Luna, A.J., Lupi, C., McCarthy, A., Ningthoujam, L., Osono, N., Peate, D.W., Persaud, P., Qiu, N., Robinson, C., Satolli, S., Sauermilch, I., Schindlbeck, J.C., Skinner, S., Straub, S., Su, X., Su, C., Tian, L., van der Zwan, F.M., Wan, S., Wu, H., Xiang, R., Yadav, R., Yi, L., Yu, P.S., Zhang, C., Zhang, J., Zhang, Y., Zhao, N., Zhong, G., and Zhong, L., 2018. Rapid transition from continental breakup to igneous oceanic crust in the South China Sea. Nature Geoscience, 11(10):782–789. **https://doi.org/10.1038/s41561-018-0198-1**

Lizarralde, D., Axen, G.J., Brown, H.E., Fletcher, J.M., González-Fernández, A., Harding, A.J., Holbrook, W.S., Kent, G.M., Paramo, P., Sutherland, F., and Umhoefer, P.J., 2007. Variation in styles of rifting in the Gulf of California. Nature, 448(7152):466–469. **https://doi.org/10.1038/nature06035**

Loreto, M.F., Zitellini, N., Ranero, C.R., Palmiotto, C., and Prada, M., 2021. Extensional tectonics during the Tyrrhenian back-arc basin formation and a new morpho-tectonic map. Basin Research, 33(1):138–158. **https://doi.org/10.1111/bre.12458**

Lustrino, M., Duggen, S., and Rosenberg, C.L., 2011. The Central-Western Mediterranean: Anomalous igneous activity in an anomalous collisional tectonic setting. Earth-Science Reviews, 104(1):1–40. **https://doi.org/10.1016/j.earscirev.2010.08.002**

MacLeod, C.J., Escartín, J., Banerji, D., Banks, G.J., Gleeson, M., Irving, D.H.B., Lilly, R.M., McCaig, A.M., Niu, Y., Allerton, S., and Smith, D.K., 2002. Direct geological evidence for oceanic detachment faulting: the Mid-Atlantic

Ridge, 15°45′N. Geology, 30(10):879–882. https://doi.org/10.1130/0091-7613(2002)030<0879:DGEFOD>2.0.CO;2
Malinverno, A., and Ryan, W.B.F., 1986. Extension in the Tyrrhenian Sea and shortening in the Apennines as result of arc migration driven by sinking of the lithosphere. Tectonics, 5(2):227–245. https://doi.org/10.1029/TC005i002p00227
Malinverno, A., Saito, S., and Vannucchi, P., 2016. Horizontal principal stress orientation in the Costa Rica Seismogenesis Project (CRISP) transect from borehole breakouts. Geochemistry, Geophysics, Geosystems, 17(1):65–77. https://doi.org/10.1002/2015GC006092
Marchesi, C., Garrido, C.J., Godard, M., Proenza, J.A., Gervilla, F., and Blanco-Moreno, J., 2006. Petrogenesis of highly depleted peridotites and gabbroic rocks from the Mayarí-Baracoa Ophiolitic Belt (eastern Cuba). Contributions to Mineralogy and Petrology, 151(6):717–736. https://doi.org/10.1007/s00410-006-0089-0
Mauffret, A., Contrucci, I., and Brunet, C., 1999. Structural evolution of the Northern Tyrrhenian Sea from new seismic data. Marine and Petroleum Geology, 16(5):381–407. https://doi.org/10.1016/S0264-8172(99)00004-5
Ménez, B., Pisapia, C., Andreani, M., Jamme, F., Vanbellingen, Q.P., Brunelle, A., Richard, L., Dumas, P., and Réfrégiers, M., 2018. Abiotic synthesis of amino acids in the recesses of the oceanic lithosphere. Nature, 564(7734):59–63. https://doi.org/10.1038/s41586-018-0684-z
Moeller, S., Grevemeyer, I., Ranero, C.R., Berndt, C., Klaeschen, D., Sallares, V., Zitellini, N., and de Franco, R., 2013. Early-stage rifting of the northern Tyrrhenian Sea Basin: Results from a combined wide-angle and multichannel seismic study. Geochemistry, Geophysics, Geosystems, 14(8):3032–3052. https://doi.org/10.1002/ggge.20180
Moeller, S., Grevemeyer, I., Ranero, C.R., Berndt, C., Klaeschen, D., Sallares, V., Zitellini, N., and de Franco, R., 2014. Crustal thinning in the northern Tyrrhenian Rift: Insights from multichannel and wide-angle seismic data across the basin. Journal of Geophysical Research: Solid Earth, 119(3):1655–1677. https://doi.org/10.1002/2013JB010431
Oufi, O., Cannat, M., and Horen, H., 2002. Magnetic properties of variably serpentinized abyssal peridotites. Journal of Geophysical Research: Solid Earth, 107(B5):EPM 3–1–EPM 3–19. https://doi.org/10.1029/2001JB000549
Peccerillo, A., 2017. Cenozoic Volcanism in the Tyrrhenian Sea Region: (Springer). https://doi.org/10.1007/978-3-319-42491-0
Pérez-Gussinyé, M., Morgan, J.P., Reston, T.J., and Ranero, C.R., 2006. The rift to drift transition at non-volcanic margins: insights from numerical modelling. Earth and Planetary Science Letters, 244(1–2):458–473. https://doi.org/10.1016/j.epsl.2006.01.059
Prada, M., Ranero, C.R., Sallares, V., Grevemeyer, I., de Franco, R., Gervasi, A., and Zitellini, N., 2020. The structure of Mediterranean arcs: New insights from the Calabrian Arc subduction system. Earth and Planetary Science Letters, 548:116480. https://doi.org/10.1016/j.epsl.2020.116480
Prada, M., Ranero, C.R., Sallarès, V., Zitellini, N., and Grevemeyer, I., 2016. Mantle exhumation and sequence of magmatic events in the Magnaghi–Vavilov Basin (Central Tyrrhenian, Italy): New constraints from geological and geophysical observations. Tectonophysics, 689:133–142. https://doi.org/10.1016/j.tecto.2016.01.041
Prada, M., Sallares, V., Ranero, C.R., Vendrell, M.G., Grevemeyer, I., Zitellini, N., and de Franco, R., 2014. Seismic structure of the Central Tyrrhenian basin: Geophysical constraints on the nature of the main crustal domains. Journal of Geophysical Research: Solid Earth, 119(1):52–70. https://doi.org/10.1002/2013JB010527
Prada, M., Sallares, V., Ranero, C.R., Vendrell, M.G., Grevemeyer, I., Zitellini, N., and de Franco, R., 2015. The complex 3-D transition from continental crust to backarc magmatism and exhumed mantle in the Central Tyrrhenian basin. Geophysical Journal International, 203(1):63–78. https://doi.org/10.1093/gji/ggv271
Ranero, C.R., and Pérez-Gussinyé, M., 2010. Sequential faulting explains the asymmetry and extension discrepancy of conjugate margins. Nature, 468(7321):294–299. https://doi.org/10.1038/nature09520
Ros, E., Pérez-Gussinyé, M., Araújo, M., Thoaldo Romeiro, M., Andrés-Martínez, M., and Morgan, J.P., 2017. Lower Crustal Strength Controls on Melting and Serpentinization at Magma-Poor Margins: Potential Implications for the South Atlantic. Geochemistry, Geophysics, Geosystems, 18(12):4538–4557. https://doi.org/10.1002/2017GC007212
Sandwell, D.T., Müller, R.D., Smith, W.H.F., Garcia, E., and Francis, R., 2014. New global marine gravity model from CryoSat-2 and Jason-1 reveals buried tectonic structure. Science, 346(6205):65–67. https://doi.org/10.1126/science.1258213
Sartori, R., 1990. The main results of ODP Leg 107 in the frame of Neogene to Recent geology of Perityrrhenian areas. In Kastens, K.A., Mascle, J., et al., Proceedings of the Ocean Drilling Program, Scientific Results. 107: College Station, TX (Ocean Drilling Program), 715–730. https://doi.org/10.2973/odp.proc.sr.107.183.1990
Sartori, R., 2005. Bedrock geology of the Tyrrhenian Sea: insight on Alpine paleogeography and magmatic evolution of the basin. In Finetti, I., CROP Project: Deep Seismic Exploration of the Central Mediterranean and Italy. Amsterdam (Elsevier), 69–80.
Sauter, D., Cannat, M., Rouméjon, S., Andreani, M., Birot, D., Bronner, A., Brunelli, D., Carlut, J., Delacour, A., Guyader, V., MacLeod, C.J., Manatschal, G., Mendel, V., Ménez, B., Pasini, V., Ruellan, E., and Searle, R., 2013. Continuous exhumation of mantle-derived rocks at the Southwest Indian Ridge for 11 million years. Nature Geoscience, 6(4):314–320. https://doi.org/10.1038/ngeo1771
Savelli, C., 1988. Late Oligocene to Recent episodes of magmatism in and around the Tyrrhenian Sea: implications for the processes of opening in a young inter-arc basin of intra-orogenic (Mediterranean) type. Tectonophysics, 146(1):163–181. https://doi.org/10.1016/0040-1951(88)90089-3
Savelli, C., 2002. Time–space distribution of magmatic activity in the western Mediterranean and peripheral orogens during the past 30 Ma (a stimulus to geodynamic considerations). Journal of Geodynamics, 34(1):99–126. https://doi.org/10.1016/S0264-3707(02)00026-1

Sawyer, D.S., Whitmarsh, R.B., Klaus, A., et al., 1994. Proceedings of the Ocean Drilling Program, Initial Reports, 149: College Station, TX (Ocean Drilling Program). **https://doi.org/10.2973/odp.proc.ir.149.1994**

Schärer, U., Kornprobst, J., Beslier, M.-O., Boillot, G., and Girardeau, J., 1995. Gabbro and related rock emplacement beneath rifting continental crust: UPb geochronological and geochemical constraints for the Galicia passive margin (Spain). Earth and Planetary Science Letters, 130(1):187–200. **https://doi.org/10.1016/0012-821X(94)00261-V**

Seyfried, W.E., Foustoukos, D.I., and Fu, Q., 2007. Redox evolution and mass transfer during serpentinization: An experimental and theoretical study at 200°C, 500bar with implications for ultramafic-hosted hydrothermal systems at Mid-Ocean Ridges. Geochimica et Cosmochimica Acta, 71(15):3872–3886. **https://doi.org/10.1016/j.gca.2007.05.015**

Seyler, M., Lorand, J.P., Dick, H.J.B., and Drouin, M., 2007. Pervasive melt percolation reactions in ultra-depleted refractory harzburgites at the Mid-Atlantic Ridge, 15° 20′N: ODP Hole 1274A. Contributions to Mineralogy and Petrology, 153(3):303–319. **https://doi.org/10.1007/s00410-006-0148-6**

Shillington, D.J., Scott, C.L., Minshull, T.A., Edwards, R.A., Brown, P.J., and White, N., 2009. Abrupt transition from magma-starved to magma-rich rifting in the eastern Black Sea. Geology, 37(1):7–10. **https://doi.org/10.1130/G25302A.1**

Shipboard Scientific Party, 1978. Site 373: Tyrrhenian Basin. In Hsü, K., Montadert, L., et al., Initial Reports of the Deep Sea Drilling Project. 42(1): Washington, DC (US Government Printing Office), 151–174. **https://doi.org/10.2973/dsdp.proc.42-1.104.1978**

The Shipboard Scientific Party, 1973. Tyrrhenian Rise: Site 132. In Ryan, W.B.F., Hsü, K.J., et al., Initial Reports of the Deep Sea Drilling Project. 13: Washington, DC (US Government Printing Office), 403–464. **https://doi.org/10.2973/dsdp.proc.13.113.1973**

Trua, T., Clocchiatti, R., Schiano, P., Ottolini, L., and Marani, M., 2010. The heterogeneous nature of the Southern Tyrrhenian mantle: evidence from olivine-hosted melt inclusions from back-arc magmas of the Marsili seamount. Lithos, 118(1–2):1–16. **https://doi.org/10.1016/j.lithos.2010.03.008**

Trua, T., Serri, G., and Marani, M.P., 2003. Lateral flow of African mantle below the nearby Tyrrhenian plate: geochemical evidence. Terra Nova, 15(6):433–440. **https://doi.org/10.1046/j.1365-3121.2003.00509.x**

Trua, T., Serri, G., and Marani, M.P., 2007. Geochemical features and geodynamic significance of the southern Tyrrhenian backarc basin. In Beccaluva, L., Bianchini, G. and Wilson, M., Cenozoic Volcanism in the Mediterranean Area. 418: (Geological Society of America). **https://doi.org/10.1130/2007.2418(11)**

Trua, T., Serri, G., and Rossi, P.L., 2004. Coexistence of IAB-type and OIB-type magmas in the southern Tyrrhenian back-arc basin: evidence from recent seafloor sampling and geodynamic implications. Memorie Descrittive della Carta Geologica d'Italia, 44:83–96.

Tucholke, B.E., Sawyer, D.S., and Sibuet, J.C., 2007. Breakup of the Newfoundland–Iberia rift. Geological Society Special Publication, 282(1):9. **https://doi.org/10.1144/SP282.2**

Warren, J.M., 2016. Global variations in abyssal peridotite compositions. Lithos, 248-251:193–219. **https://doi.org/10.1016/j.lithos.2015.12.023**

Whitmarsh, R.B., Minshull, T.A., Russell, S.M., Dean, S.M., Louden, K.E., and Chian, D., 2001. The role of syn-rift magmatism in the rift-to-drift evolution of the West Iberia continental margin: geophysical observations. In Wilson, R.C.L., Whitmarsh, R.B., Taylor, B. and Froitzheim, N., Non-Volcanic Rifting of Continental Margins: A Comparison of Evidence from Land and Sea. 187: (Geological Society of London). **https://doi.org/10.1144/GSL.SP.2001.187.01.06**

# Site summaries

## Site TYR-1A

| | |
|---|---|
| Priority: | Alternate of TYR-07A |
| Position: | 40.00085°N, 10.994272°E<br>Cornaglia Terrace |
| Water depth (m): | 2675 |
| Target drilling depth (mbsf): | 234 |
| Approved maximum penetration (mbsf): | Discretion of shipboard party to deepen the hole if time is available |
| Survey coverage (track map; seismic profile): | Medoc6_43000-50600.sgy (CDP 47870) |
| Objective(s): | Recovery of basalts underneath Pliocene–Quaternary sediments and Messinian deposits |
| Coring program: | Hole A: RCB to total depth |
| Downhole measurements program: | Hole A: Wireline log with triple combo, FMS-sonic |
| Nature of rock anticipated: | 134 m of terrigenous sand/silt/clay over a possible 30 m of Messinian gypsum plus 70 m of basalts |

## Site TYR-02A

| | |
|---|---|
| Priority: | Primary |
| Position: | 40.00036°N, 13.407784°E<br>Campania Terrace |
| Water depth (m): | 2813 |
| Target drilling depth (mbsf): | 530 |
| Approved maximum penetration (mbsf): | Discretion of shipboard party to deepen the hole if time is available |
| Survey coverage (track map; seismic profile): | Medoc6_12750-20050.sgy CDP14890 |
| Objective(s): | The basement underneath the Pliocene–Quaternary sediments and Messinian deposits |
| Coring program: | Hole A: RCB to total depth |
| Downhole measurements program: | Hole A: Wireline log with triple combo, FMS-sonic |
| Nature of rock anticipated: | Terrigenous sand/silt/clay in the first 227 m and 233 m of Messinian gypsum plus 70 m of basalts |

## Site TYR-03A

| | |
|---|---|
| Priority: | Alternate of TYR-09A |
| Position: | 40.18388°N, 12.6413°E<br>Vavilov Basin |
| Water depth (m): | 3533 |
| Target drilling depth (mbsf): | 360 |
| Approved maximum penetration (mbsf): | Discretion of shipboard party to deepen the hole if time is available |
| Survey coverage (track map; seismic profile): | Medoc9_2200-11000.sgy CDP 7599 |
| Objective(s): | Serpentinized peridotite |
| Coring program: | Hole A: RCB to total depth<br>Hole B: APC/XCB from the deepest 50 m of sediments plus 5 m into the basement |
| Downhole measurements program: | Hole A: Wireline log with triple combo, FMS-sonic |
| Nature of rock anticipated: | Terrigenous sand/silt/clay in the first 220 m followed by 140 m of serpentinized peridotite |

## Site TYR-04A

| | |
|---|---|
| Priority: | Alternate of TYR-10A |
| Position: | 40.18402°N, 12.72801°E<br>Vavilov Basin |
| Water depth (m): | 3546 |
| Target drilling depth (mbsf): | 548 |
| Approved maximum penetration (mbsf): | Discretion of shipboard party to deepen the hole if time is available |
| Survey coverage (track map; seismic profile): | Medoc9_2200-11000.sgy CDP 6417 |
| Objective(s): | Exhumed mantle rocks |
| Coring program: | Hole A: RCB to total depth<br>Hole B: APC/XCB from the deepest 50 m of sediments plus 5 m into the basement |
| Downhole measurements program: | Hole A: Wireline log with triple combo, FMS-sonic |
| Nature of rock anticipated: | Terrigenous sand/silt/clay in the first 478 m above exhumed mantle rocks plus 70 m of serpentinized peridotite |

## Site TYR-05A

| | |
|---|---|
| Priority: | Alternate of TYR-11A |
| Position: | 40.26609°N, 12.69432°E<br>Vavilov Basin |
| Water depth (m): | 3530 |
| Target drilling depth (mbsf): | 228 |
| Approved maximum penetration (mbsf): | Discretion of shipboard party to deepen the hole if time is available |
| Survey coverage (track map; seismic profile): | Medoc8_35250-43000.sgy CDP 39599 |
| Objective(s): | Exhumed mantle rocks |
| Coring program: | Hole A: RCB to total depth<br>Hole B: APC/XCB from the deepest 50 m of sediments plus 5 m into the basement |
| Downhole measurements program: | Hole A: Wireline log with triple combo, FMS-sonic |
| Nature of rock anticipated: | Terrigenous sand/silt/clay in the first 88 m, plus 140 m of exhumed mantle rocks |

## Site TYR-07A

| | |
|---|---|
| Priority: | Primary |
| Position: | 40.00097°N, 10.98622°E<br>Cornaglia Terrace |
| Water depth (m): | 2700 |
| Target drilling depth (mbsf): | 265 |
| Approved maximum penetration (mbsf): | Discretion of shipboard party to deepen the hole if time is available |
| Survey coverage (track map; seismic profile): | Medoc6_43000-50600.sgy CDP 47980 |
| Objective(s): | The basement underneath Pliocene–Quaternary sediments and Messinian deposits |
| Coring program: | Hole A: RCB to total depth |
| Downhole measurements program: | Hole A: Wireline log with triple combo, FMS-sonic |
| Nature of rock anticipated: | Terrigenous sand/silt/clay in the first 147 m and possibly about 48 m of Messinian gypsum plus 70 m of basalts |

## Site TYR-08A

| | |
|---|---|
| Priority: | Alternate of TYR-2A |
| Position: | 40.00036°N, 13.385832°E<br>Campania Terrace |
| Water depth (m): | 2837 |
| Target drilling depth (mbsf): | 524 |
| Approved maximum penetration (mbsf): | Discretion of shipboard party to deepen the hole if time is available |
| Survey coverage (track map; seismic profile): | Medoc6_12750-20050.sgy CDP 14990 |
| Objective(s): | The basement underneath the Pliocene–Quaternary sediments and Messinian deposits |
| Coring program: | Hole A: RCB to total depth |
| Downhole measurements program: | Hole A: Wireline log with triple combo, FMS-sonic |
| Nature of rock anticipated: | Terrigenous sand/silt/clay in the first 244 m and 210 m of Messinian gypsum plus 70 m of basalts |

## Site TYR-09A

| | |
|---|---|
| Priority: | Primary |
| Position: | 40.18388°N, 12.63243°E<br>Abyssal plain of Vavilov Basin |
| Water depth (m): | 3533 |
| Target drilling depth (mbsf): | 418 |
| Approved maximum penetration (mbsf): | Discretion of shipboard party to deepen the hole if time is available |
| Survey coverage (track map; seismic profile): | Medoc9_2200-11000.sgy (CDP 7720) |
| Objective(s): | Recovery of serpentinized peridotite underneath Pliocene–Quaternary sediments |
| Coring program: | Hole A: RCB to total depth<br>Hole B: APC/XCB from the deepest 50 m of sediments plus 5 m into the basement |
| Downhole measurements program: | Hole A: Wireline log with triple combo, FMS-sonic |
| Nature of rock anticipated: | 278 m of terrigenous sand/silt/clay followed by 140 m of serpentinized peridotites |

## Site TYR-10A

| | |
|---|---|
| Priority: | Primary |
| Position: | 40.18398°N, 12.70826°E<br>Vavilov Basin |
| Water depth (m): | 3544 |
| Target drilling depth (mbsf): | 435 |
| Approved maximum penetration (mbsf): | Discretion of shipboard party to deepen the hole if time is available |
| Survey coverage (track map; seismic profile): | Medoc9_2200-11000.sgy (CDP 6686) |
| Objective(s): | Recovery of serpentinized peridotites underneath Pliocene–Quaternary sediments deposits |
| Coring program: | Hole A: RCB to total depth<br>Hole B: APC/XCB from the deepest 50 m of sediments plus 5 m into the basement |
| Downhole measurements program: | Hole A: Wireline log with triple combo, FMS-sonic |
| Nature of rock anticipated: | 365 m of terrigenous sand/silt/clay followed by 70 m of serpentinized mantle rocks |

## Site TYR-11A

| | |
|---|---|
| Priority: | Primary |
| Position: | 40.26614°N, 12.70529°E<br>Vavilov Basin |
| Water depth (m): | 3538 |
| Target drilling depth (mbsf): | 342 |
| Approved maximum penetration (mbsf): | Discretion of shipboard party to deepen the hole if time is available |
| Survey coverage (track map; seismic profile): | Medoc8_35250-43000.sgy (CDP 39749) |
| Objective(s): | Recovery of serpentinized peridotite underneath Pliocene–Quaternary sediments deposits |
| Coring program: | Hole A: RCB to total depth<br>Hole B: APC/XCB from the deepest 50 m of sediments plus 5 m into the basement |
| Downhole measurements program: | Hole A: Wireline log with triple combo, FMS-sonic |
| Nature of rock anticipated: | 202 m of terrigenous sand/silt/clay followed by 140 m into the serpentinized mantle peridotite |

## Site TYR-12A

| | |
|---|---|
| Priority: | Primary |
| Position: | 40.4159°N, 12.7076°E<br>Abyssal plain of Vavilov Basin |
| Water depth (m): | 3590 |
| Target drilling depth (mbsf): | 723 |
| Approved maximum penetration (mbsf): | Discretion of shipboard party to deepen the hole if time is available |
| Survey coverage (track map; seismic profile): | Medoc11_8250-15750.sgy (CDP 12198) |
| Objective(s): | Recovery of peridotite underneath Pliocene–Quaternary sediments deposits |
| Coring program: | Hole A: APC/XCB of the whole sedimentary cover plus 5 m into the basement<br>Hole B: RCB from the deepest 50 m of sediment to total depth |
| Downhole measurements program: | Hole B: Wireline log with triple combo, FMS-sonic |
| Nature of rock anticipated: | 653 m of terrigenous sand/silt/clay followed by 70 m of serpentinized mantle rocks |

## Site TYR-13B

| | |
|---|---|
| Priority: | Alternate of TYR-7A |
| Position: | 40.001003°N, 10.95549°E<br>Cornaglia Terrace |
| Water depth (m): | 2713 |
| Target drilling depth (mbsf): | 380 |
| Approved maximum penetration (mbsf): | Discretion of shipboard party to deepen the hole if time is available |
| Survey coverage (track map; seismic profile): | Medoc6_43000-50600.sgy (CDP 48400) |
| Objective(s): | Recovery of basalts underneath Pliocene–Quaternary sediments and Messinian deposits |
| Coring program: | Hole A: RCB to total depth |
| Downhole measurements program: | Hole A: Wireline log with triple combo, FMS-sonic |
| Nature of rock anticipated: | 200 m of terrigenous sand/silt/clay over about 110 m of Messinian gypsum followed by 70 m of basalts |

## Site TYR-14A

| | |
|---|---|
| Priority: | Alternate of TYR-02A |
| Position: | 39.71273°N, 13.31500°E<br>Campania Terrace |
| Water depth (m): | 3381 |
| Target drilling depth (mbsf): | 566 |
| Approved maximum penetration (mbsf): | Discretion of shipboard party to deepen the hole if time is available |
| Survey coverage (track map; seismic profile): | M2A4_TYR-14A_CDP500-2100.sgy (CDP 5963);<br>M30_TYR14A_CDP10750-12700.sgy (CDP 11626) |
| Objective(s): | Recovery of basalts underneath Pliocene–Quaternary sediments deposits |
| Coring program: | Hole A: RCB to total depth |
| Downhole measurements program: | Hole A: Wireline log with triple combo, FMS-sonic |
| Nature of rock anticipated: | 496 m of terrigenous sand/silt/clay followed by 70 m of basalts |

## Site TYR-15A

| | |
|---|---|
| Priority: | Alternate of TYR-09A |
| Position: | 40.18420°N, 12.56710°E<br>Vavilov Basin |
| Water depth (m): | 3600 |
| Target drilling depth (mbsf): | 315 |
| Approved maximum penetration (mbsf): | Discretion of shipboard party to deepen the hole if time is available |
| Survey coverage (track map; seismic profile): | Medoc9_2200-11000.sgy (CDP 8610) |
| Objective(s): | Recovery of peridotite underneath Pliocene–Quaternary sediments deposits |
| Coring program: | Hole A: RCB to total depth<br>Hole B: APC/XCB from the deepest 50 m of sediments plus 5 m into the basement |
| Downhole measurements program: | Hole A: Wireline log with triple combo, FMS-sonic |
| Nature of rock anticipated: | 175 m of terrigenous sand/silt/clay plus 140 m of serpentinized peridotites |

## Site TYR-16A

| | |
|---|---|
| Priority: | Alternate of TYR-10A |
| Position: | 40.18387°N, 12.67717°E<br>Vavilov Basin |
| Water depth (m): | 3578 |
| Target drilling depth (mbsf): | 341 |
| Approved maximum penetration (mbsf): | Discretion of shipboard party to deepen the hole if time is available |
| Survey coverage (track map; seismic profile): | Medoc9_2200-11000.sgy (CDP 7110) |
| Objective(s): | Recovery of peridotite underneath Pliocene–Quaternary sediments deposits |
| Coring program: | Hole A: RCB to total depth<br>Hole B: APC/XCB from the deepest 50 m of sediments plus 5 m into the basement |
| Downhole measurements program: | Hole A: Wireline log with triple combo, FMS-sonic |
| Nature of rock anticipated: | 271 m of terrigenous sand/silt/clay plus 70 m of exhumed mantle rocks |

## Site TYR-17A

| | |
|---|---|
| Priority: | Alternate of TYR-11A |
| Position: | 40.33121°N, 12.67304°E<br>Abyssal plain of Vavilov Basin |
| Water depth (m): | 3600 |
| Target drilling depth (mbsf): | 602 |
| Approved maximum penetration (mbsf): | Discretion of shipboard party to deepen the hole if time is available |
| Survey coverage (track map; seismic profile): | M29B_TYR17A_CDP12361-14750.sgy (CDP 13010);<br>ST04_TYR17A_CDP500-1600.sgy (CDP 995) |
| Objective(s): | Recovery of mantle rocks underneath Pliocene–Quaternary sediments deposits |
| Coring program: | Hole A: RCB to total depth<br>Hole B: APC/XCB from the deepest 50 m of sediments plus 5 m into the basement |
| Downhole measurements program: | Hole A: Wireline log with triple combo, FMS-sonic |
| Nature of rock anticipated: | 462 m of terrigenous sand/silt/clay followed by 140 m of serpentinized peridotites |

## Site TYR-18A

| | |
|---|---|
| Priority: | Alternate of TYR-12A |
| Position: | 40.41600°N, 12.74424°E<br>Vavilov Basin |
| Water depth (m): | 3600 |
| Target drilling depth (mbsf): | 691 |
| Approved maximum penetration (mbsf): | Discretion of shipboard party to deepen the hole if time is available |
| Survey coverage (track map; seismic profile): | Medoc11_8250-15750.sgy (CDP 12696);<br>ST03A_TYR19A_CDP4228-5132.sgy (CDP 4640) |
| Objective(s): | Recovery of peridotite underneath Pliocene–Quaternary sediments deposits |
| Coring program: | Hole A: APC/XCB of the whole sedimentary cover plus 5 m into the basement<br>Hole B: RCB from the deepest 50 m of sediment to total depth |
| Downhole measurements program: | Hole B: Wireline log with triple combo, FMS-sonic |
| Nature of rock anticipated: | 621 m of terrigenous sand/silt/clay plus 70 m of serpentinized peridotites |

## Site TYR-19A

| | |
|---|---|
| Priority: | Alternate of TYR-12A |
| Position: | 40.38562°N, 12.74428°E<br>Vavilov Basin |
| Water depth (m): | 3601 |
| Target drilling depth (mbsf): | 1133 |
| Approved maximum penetration (mbsf): | Discretion of shipboard party to deepen the hole if time is available |
| Survey coverage (track map; seismic profile): | M29B_TYR17A_CDP12361-14750.sgy (CDP 13690);<br>ST03A_TYR19A_CDP4228-5132.sgy (CDP 4535) |
| Objective(s): | Recovery of peridotite underneath Pliocene–Quaternary sediments deposits |
| Coring program: | Hole A: APC/XCB of the whole sedimentary cover plus 5 m into the basement<br>Hole B: RCB from the deepest 50 m of sediment to total depth |
| Downhole measurements program: | Hole B: Wireline log with triple combo, FMS-sonic |
| Nature of rock anticipated: | 1063 m of terrigenous sand/silt/clay plus 70 m of serpentinized mantle rocks |

## Site TYR-20A

| | |
|---|---|
| Priority: | Alternate of TYR-02A |
| Position: | 39.999778°N, 13.5958344°E<br>Campania Terrace |
| Water depth (m): | 2698 |
| Target drilling depth (mbsf): | 470 |
| Approved maximum penetration (mbsf): | Discretion of shipboard party to deepen the hole if time is available |
| Survey coverage (track map; seismic profile): | Medoc6_TYR20A_CDP10200-14600.sgy (CDP 12320) |
| Objective(s): | Recovery of basalts underneath Pliocene–Quaternary sediments deposits |
| Coring program: | Hole A: RCB to total depth |
| Downhole measurements program: | Hole A: Wireline log with triple combo, FMS-sonic |
| Nature of rock anticipated: | 400 m of terrigenous sand/silt/clay, plus 70 m of basalts |

## Site TYR-21A

| | |
|---|---|
| Priority: | Alternate of TYR-09A |
| Position: | 40.001163°N, 11.62511°E<br>Magnaghi Basin |
| Water depth (m): | 3366 |
| Target drilling depth (mbsf): | 409 |
| Approved maximum penetration (mbsf): | Discretion of shipboard party to deepen the hole if time is available |
| Survey coverage (track map; seismic profile): | Medoc6_TYR21A_CDP36250-41950.sgy (CDP 39250) |
| Objective(s): | Recovery of basalts underneath Pliocene–Quaternary sediments deposits |
| Coring program: | Hole A: RCB to total depth<br>Hole B: APC/XCB from the deepest 50 m of sediments plus 5 m into the basement |
| Downhole measurements program: | Hole A: Wireline log with triple combo, FMS-sonic |
| Nature of rock anticipated: | 269 m of terrigenous sand/silt/clay, plus 140 m of serpentinized mantle peridotites |